DRA

E. Chipman, A/EZ-7

AS&E

American Science
and Engineering, Inc.
Fort Washington
Cambridge, Massachusetts 02139
617-868-1614 Telex 921-458

APRIL 1983

ASE-4702

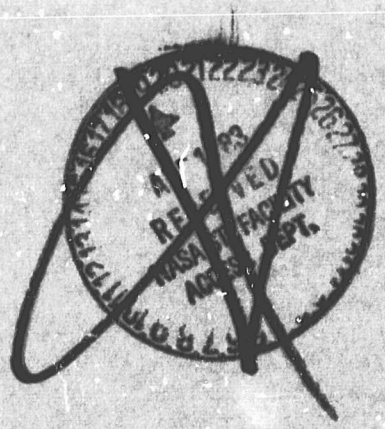

FINAL REPORT

AN INVESTIGATION OF CORONAL ACTIVE REGION LOOP STRUCTURES USING AS&E ROCKET X-RAY IMAGES

CONTRACT NASW-3586

PERIOD OF PERFORMANCE:
31 MARCH 1982
TO
31 MARCH 1983

PREPARED FOR:
NATIONAL AERONAUTICS
AND SPACE ADMINISTRATION
WASHINGTON, D.C. 20546

ASE-4792

FINAL REPORT

CONTRACT NASW-3586

AN INVESTIGATION OF CORONAL ACTIVE REGION LOOP STRUCTURES USING AS&E ROCKET X-RAY IMAGES

Prepared by: American Science & Engineering, Inc.
Fort Washington
Cambridge, Mass. 02139

Prepared for: National Aeronautics and Space Administration
Washington, D.C. 20546

Period of Performance: 31 March 1982 to 31 March 1983

Date of Report: April 1983

David F. Webb
Principal Investigator

Allen S. Krieger
Vice President
Space Systems Division

TABLE OF CONTENTS

FOREWORD

This document is the final report for work performed under NASA contract NASW-3586. The overall goal of the contract was to study the coronal structure of active region loops.

Under this contract AS&E was to furnish the personnel, services, materials, facilities and equipment to complete the work effort. The original contract was amended by AS&E letter MEG-82-164, dated 26 April 1982, to authorize the use of the facilities accountable to NASA contract NAS 8-32671(F) on a no-charge, non-interference basis in support of contract NASW-3586.

This effort was performed at AS&E under the direction of David F. Webb, Principal Investigator.

1.0 INTRODUCTION

1.1 Statement of Work

The scientific objective of this contract was to gain an improved understanding of the coronal structure of active region loops through the analysis of X-ray images from AS&E sounding rocket flights. The level of effort originally proposed in AS&E document 4622 dated 10 April 1981 was descoped in AS&E letter MEG-81-355 dated 8 October 1981. This amended Statement of Work was to achieve the scientific objective in two phases of effort:

- Study the detailed structure and plasma properties of active region loops using simultaneous high resolution, aligned X-ray images, magnetograms, Hα images, and VLA microwave radio maps. The derived parameters will be compared to models of microwave emission processes and will be used to estimate the magnetic strengths in loops.

- Model the emission measure-temperature distribution within the coronal loops using soft X-ray images of high spatial resolution and Aerospace SOLEX X-ray data of high spectral resolution. These distributions will then be used to test various coronal loop models.

The program was further amended in AS&E letter MEG-81-432 dated 2 December 1981 to add an extended period for Fiscal Years 1983 and 1984 at NASA's option. However, this option was not exercised by NASA. Phase two of the amended Statement of Work required comparison of the soft X-ray rocket imagery with near-simultaneous X-ray spectroscopic data obtained by the Aerospace Corporation's SOLEX experiment on board the P78-1 satellite. We had expected these data to be available during the times of AS&E rocket flights in November 1979 and on 13 February 1981. Unfortunately, for these dates the SOLEX data were either unavailable or unsuitable for our purposes.

Because of the lack of data sufficient to complete phase two, we substituted several studies which were originally part of the extended plan and were related to the scientific objective. These were to: (1) study the development of coronal holes as a function of the solar cycle, and to investigate the physics of coronal holes and their boundaries by comparison of X-ray images with He I-10830 Å images, and (2) study the physics of a post-flare loop system on 7 November 1979 by determining the plasma and magnetic field parameters of the loop through a comparison of microwave and X-ray observations. These phases of the contract were accomplished successfully during the period of performance.

1.2 Summary of Scientific Results

Phase one work completed during the contract included a comparative study of the most intense sources of centimetric emision in two active regions to coronal loops, sunspots, chromospheric structures and photospheric magnetic fields. This study used simultaneous, high spatial resolution observations at 6 cm, in soft X-rays, in photospheric magnetograms and in optical filtergrams. A principal result was that a majority of the bright microwave components were not associated with sunspots or with X-ray emission.

In this and related studies the X-ray and magnetic field observations were used to constrain possible mechanisms for the centimetic radio emission. Thermal gyroresonance absorption was consistent with some of the observations, but a major and unexpected result was that a nonthermal mechanism appeared necessary to explain the brightest microwave components. This result suggests that discrete regions of continuous particle acceleration may be common in active regions. These results are described in a paper that has been accepted for publication and is reproduced in Section 4.1.

Following this study digital arrays of the X-ray images obtained with two filters on 7 and 16 November 1979 were reduced to energy flux arrays and two-dimensional maps of emission measure and electron temperature were produced. This reduction used standard techniques (e.g., Davis et al., 1975; Vaiana et al., 1977) of film calibration, image coalignment, density-to-energy conversion, and deconvolution to remove the mirror

point spread function from the energy arrays. For 16 November 1979 the deconvolution was more difficult and time consuming because the kanigen metal mirror has broad scattering characteristics and its point response function has only been measured at one wavelength.

Results for 16 November indicate that one of the two active regions studied had an integrated emission measure of 6×10^{46} cm^{-5}, equivalent to that derived by Davis et al. (1975) for a similar small region. The brightest X-ray loop in the active region, a type of loop called a penumbral loop by Webb and Zirin (1981), had an average density of 2×10^{10} cm^{-3} and a temperature of 3.3×10^{6}K. The plasma parameters of this and 3 other loops emitting in both X-rays and microwaves imply that the radio emission is consistent with gyro-resonance absorption at the third and fourth harmonic, at least from part of each loop. This analysis in continuing and will result in a paper to be submitted to a scientific journal.

On 7 November 1979 a post-flare loop system was observed in X-rays, 6 cm radio and H-alpha. The X-ray flare structure consisted of an extended loop system of length 2 arc-min and average temperature about 8×10^{6}K. Comparison of these data indicate that the peak microwave emission occurred in loops lying under the X-ray loops. Because the X-ray loop was so extended we could examine the two-dimensional distribution of opacity and of Θ, the angle between the magnetic field direction and the line of sight, to provide a detailed test of radio emission mechanisms in the loop. An abstract of these results, which will be presented at a scientific meeting in June 1983, appears in Section 2.1. A paper is also being prepared.

During the period of performance two studies involving the development of coronal holes as a function of the solar cycle were completed. The first used co-temporal AS&E X-ray and KPNO HeI-10830 Å images to compare coronal hole boundaries from 1974 to 1981. There was good agreement between the two wavelengths for large area holes, but poor agreement for mid and low-latitude holes of small area. The results indicate that the contrast between holes and large-scale coronal structure decreases toward solar maximum, and that the distinction between open and closed

magnetic field regions is not as sharp as previously thought. These results are described in a paper which has been accepted for publication and is reproduced in Section 4.2.

Finally, we have completed a study of the polar evolution of the solar magnetic field around sunspot maximum, when the net polar flux reverses polarity and coronal holes redevelop at the poles. This hole redevelopment was compared with the poleward migration of the photospheric field and of the polar crown of filaments using rocket and satellite X-ray and EUV images, and ground-based synoptic Hα , white light, HeI-10830 Å and photospheric magnetogram data. We found that the appearance of mid-latitude holes which expand to encircle the poles, the peak of flux emergence at low latitudes, and the polar polarity reversal all occurred within a few solar rotations. The polar crown disappeared and the polar holes redeveloped about 6 mo. to 1 1/2 years afterward. Some significant complications were found when these results were compared to Babcock-type models of the solar cycle. These results are discussed in a paper which will be submitted to Solar Physics shortly. A preliminary report on this work was presented by Webb and Davis (1981). A preliminary version of the paper is reproduced in Section 4.3.

1.3 References

Davis, J.M., Gerassimenko, M., Krieger, A.S. and Vaiana, G.S. 1975, Solar Phys. 45, 393.

Vaiana, G.S., Van Speybroeck, L., Zombeck, M.V., Krieger, A.S., Silk, J.K., and Timothy, A.: 1977, Space Sci. Instru. 3, 19.

Webb, D.F. and Zirin, H.: 1981, Solar Phys. 69, 99.

Webb, D.F. and Davis, J.M.: 1981, B.A.A.S. 13, 906.

2.0 PRESENTATIONS AND PUBLICATIONS

The results of the work performed under this contract have been or will be presented to the scientific community in the form of a presentation and as papers submitted or published in scientific journals. The abstract of the presentation appears below and the papers are reproduced in Section 4.0.

2.1 Presentation

The Spatial Distribution of 6 cm Gyroresonance Emission From a Flaring X-ray Loop

To be presented by D.F. Webb with J.M. Davis, S. Kahler and M. Kundu at a meeting of the Solar Physics Division of the AAS in Pasadena, CA from 22-24 June 1983.

We compare simultaneous high resolution soft X-ray and 6 cm images of a flaring region to deduce the microwave emission mechanisms in that region. The photographic X-ray images were obtained from an AS&E sounding rocket payload flown on 7 November 1979. At 2050 UT the decay phase of an M3 X-ray flare in Hale Region 16413 was observed. During this time 6 cm observations of the region were made with the VLA. Synthesis maps of radio brightness temperature with a spatial resolution of about 5 arc sec were then obtained. The X-ray images were converted to deconvolved energy arrays which were used to obtain line-of-sight emission integrals and average temperatures throughout the region. The X-ray flare structure consisted of a large loop system of length ~ 2 arc min and average temperature $\sim 8 \times 10^6$ K. Comparison of these data to the aligned radio image showed that the peak 6 cm emission appeared to come from a region below the X-ray loop. The predicted 6 cm flux due to thermal bremsstrahlung calculated on the basis of the X-ray parameters was about an order of magnitude less than the observed flux. We model the loop geometry to examine emission expected from gyroresonance absorption along the loop. Since the loop presents a wide range of angles between the presumed magnetic field direction and the line of sight, and gyroresonance emission is strongly dependent on this angle, these data provide a stringent test of this mechanism.

2.2 Publications

Webb, D.F., Davis, J.M.. Kundu, M.R. and Velusamy, T.: 1983, "X-ray and Microwave Observations of Active Regions", Solar Phys. (in press).

Kahler, S., Davis, J.M. and Harvey, J.W.: 1983, "Comparision of Coronal Holes Observed in Soft X-rays and HeI-10830 Å Spectroheliograms," Solar Phys. (in press).

Webb, D.F., Davis, J.M. and McIntosh, P.S.: 1983, "The Reappearance of Polar Coronal Holes and the Evolution of the Solar Magnetic Field," Solar Phys. (to be submitted).

3.0 PERSONNEL AND ACKNOWLEDGEMENTS

David Webb was the Principal Investigator on the contract and directed the program. Stephen Kahler made significant contributions to the research effort. We are grateful to John Davis for his assistance with the rocket data and helpful guidance. Dr. Davis is PI of the AS&E X-ray Astronomy Rocket Program. We also thank Allen Krieger, Vice President of AS&E's Space Systems Division, for his assistance.

We acknowledge the work of the AS&E Technical Publications Dept., especially Michael Rizza for his careful photographic work.

4.0 SCIENTIFIC RESULTS

4.1 X-ray and Microwave Observations of Active Regions

D.F. Webb and J.M. Davis

American Science and Engineering, Inc.
Cambridge, Mass.

and

M.R. Kundu and T. Velusamy

University of Maryland
College Park, MD

ASE-4702-A

"X-RAY AND MICROWAVE OBSERVATIONS OF ACTIVE REGIONS"

by D.F. Webb and J.M. Davis

American Science and Engineering, Inc.,

Cambridge, MA 02139, USA

and

M.R. Kundu and T. Velusamy†

Astronomy Program,

University of Maryland, College Park, MD 20742, USA

To be Published in SOLAR PHYSICS

March 1982

Revised: October 1982

†Presently at the Tata Institute of Fundamental Research, Bombay, India

ABSTRACT

We compare coordinated, high spatial resolution (2-3 arc-sec) observations at 6 cm and in soft X-rays with photospheric magnetograms and optical filtergrams of two active regions. The correspondence of the brightest centimetric components in these regions with coronal loops, sunspots and pores, chromospheric structures and the photospheric magnetic field was determined. Our principal results are: The association between the microwave components and coronal X-ray and photospheric magnetic field structures is complex; in general X-ray emission was not associated with the microwave components. A majority of the components were not associated with sunspots, although the brightest ($T_b > 4 \times 10^6$ K) components overlay regions of strong photospheric field or high field gradients. Several of the components coincided with the apparent bases of shorter coronal loops and 4 with the tops of X-ray loops.

The X-ray and magnetic field observations are used to constrain possible centimetric emission mechanisms. Thermal bremsstrahlung can not be a significant contributor to this bright microwave emission. Thermal gyro-resonance absorption is consistent with some of the observations, but untenable for those components which are bright in microwaves, lack X-ray emission, and overlie regions of weak magnetic field. As an explanation for the brightest ($T_b > 4 \times 10^6$ K) components, the g-r theory requires coronal loops with significant currents but very low densities. Alternatively, a nonthermal mechanism implies that the emission arises from the transition region and suggests that discrete regions of continuous particle acceleration may be common in active regions.

1. INTRODUCTION

Much recent work in solar physics has focussed on the problem of the structure of active regions (ARs) in the transition region and low corona. This study has been paced by observations from rockets and satellites, which can observe X-ray and EUV emission with high spatial and spectral resolution, and with large ground-based arrays at centimeter radio wavelengths. The high spatial resolution (a few arc-sec) of the instruments has substantially altered our view of the transition region and corona, and prompted the development of more realistic models of active regions.

The slowly varying component of the radio emission over ARs has a spectral maximum at centimeter wavelengths. Only recently has this emission been examined with sensitivity and spatial resolution approaching that of other wavelengths. Observations have shown that the brightest centimetric components are associated with structures near sunspots, transverse fields over neutral lines or filaments (Kundu et al., 1977; 1980; 1981), and emerging flux regions (Kundu and Velusamy, 1980). The fact that these latter features are also associated with X-ray loops and that thermal bremsstrahlung can produce emission at both microwave and X-ray wavelengths leads us to suspect that at least part of the microwave emission in active regions arises in coronal loops. Recent high resolution centimeter observations with the Very Large Array (VLA) have revealed loop-like structures reminiscent of those observed in X-rays and EUV (Kundu and Velusamy, 1980). Previous comparisons of imaging observations in soft X-rays and microwaves have shown that most of the general plage-related emission in ARs is due to thermal bremsstrahlung (Gerassimenko et al., 1976; Pallavicini et al., 1979). The brighter

centimetric components require an explanation in terms of low harmonic gyromagnetic emission (e.g., Kundu et al., 1980; Alissandrakis et al., 1980; Felli et al., 1981).

This paper presents the initial results of a long term study whose purpose is to measure the plasma parameters and the properties of the magnetic field in coronal structures through the use of combined high spatial resolution X-ray, magnetogram and microwave data. Although this first paper is primarily observational, the results are sufficient to constrain possible centimetric emission mechanisms. In particular we conjecture that the results imply a significant small-scale, nonthermal component to the slowly varying radiation from ARs.

We describe the analysis of two active regions observed on 16 November 1979. The data include soft X-ray filtergrams from a sounding rocket flight, microwave radio maps of total intensity and circular polarization obtained with the VLA, photospheric magnetograms and optical filtergrams, all of comparable high spatial resolution (1-3 arcsec). This is the first time that such coordinated, high spatial resolution observations in microwaves and X-rays of active regions have been available. In the next section we describe the observational data. In Section 3 we discuss the observational results. The key results are summarized in Section 4 and discussed in the last section.

2. THE OBSERVATIONS AND DATA ANALYSIS

2.1 Soft X-ray Data

On 16 November 1979 American Science and Engineering (AS&E) launched the second of two rocket flights designed to obtain a complete view of the solar corona at solar maximum. The payload utilized a

metallic mirror previously flown many times (Vaiana et al., 1973). Full-disk images of the corona with an on-axis spatial resolution of 2-3 arc-sec were obtained between 1702 and 1705 UT. The images were recorded with two Kodak emulsions, SO-212, a moderate-speed emulsion, and SO-253, a fine-grain holographic emulsion which permits improved definition of coronal features (Davis et al., 1979).

2.2 Microwave Data

The radio observations were made at 6 cm with the VLA of the National Radio Astronomy Observatory between 1500 and 1645 UT on 16 November 1979. Seventeen antennas were available during the observations, providing good determination of the two-dimensional brightness distribution. The system was sensitive to structures smaller than 3 arc-min because the shortest spacing used for these maps was 1200 λ. The observing procedure and calibration and cleaning methods were similar to those discussed by Kundu and Velusamy (1980). The observations alternated between two active regions, Hale Nos. 16419 and 16421. The centers of the regions used for continuous tracking were located at N10W23 and N32W33 in heliographic coordinates at 00 UT. Synthesized maps of total intensity and circular polarization were obtained of a field of view of 6.4 x 6.4 arc-min around each active region. The synthesized beam was 3 x 6 arc-sec with the long axis oriented in the north-south direction. The dynamic range on these maps was greater than a factor of 10.

2.3 Chromospheric and Photospheric Data

Full-disk photospheric magnetograms were obtained at Kitt Peak National Observatory (KPNO). The magnetograms used for our study were obtained at 1543, 1743, 1828, 1917, 2007, and 2100 UT. In addition, a

full disk He I - 10830 Å filtergram was obtained at KPNO at 1647 UT. The magnetograms at 1543 and 1743 UT bracketed the times of the X-ray and radio observations and therefore were used in our detailed analysis. No significant changes in the general magnetic field in either of the two ARs was observed on the magnetograms. In addition, video magnetograph (VMG) images were obtained from Big Bear Solar Observatory (BBSO) and used to verify the KPNO data.

Chromospheric data were obtained in collaboration with BBSO. Nearly continous H_α observations with time resolution of 10 sec of both active regions were obtained on 16 November from 1555 to 2200 UT. Most of these images were centered on H419; only 5 minutes of high resolution data were taken of H421 starting at 2154 UT. A cine version of these data was used to select individual frames for enlargment and to study the evolution of chromospheric and photospheric structures in H419. Frames enlarged for the detailed study were recorded at 1658, 1935 and 1937 UT in H_α, H_α wings and continuum, respectively, and in H_α at 2157 UT for H421. Full-disk patrol H_α data obtained at 1937 UT (H_α) and 2140 UT (near-H_α continuum) were used in the alignment scheme.

2.4 Method of Comparison

A selection of the X-ray and visible light images, the microwave maps, and the optical images were converted to transparencies with a scale of 4.8 arc-sec mm^{-1} (40.6 cm solar disk diameter). To compare the locations of the X-ray and microwave features, the heliographic positions of the centroids of the sunspots that lay within the field of the radio maps were determined, using a Mt. Wilson sunspot chart and an H_α image from NOAA-Boulder. These positions were converted to celestial coordinates at 1700 UT and plotted on the radio maps. Visible light

images from the AS&E experiment revealed sunspots which were used as an intermediary to coalign the X-ray, radio and optical data. The magnetograms were coaligned by using the fact that H_α plage emission tends to occur in areas of strong vertical magnetic fields. Up to 6 spot groups were used for alignment. The alignment accuracy between the X-ray data and the radio maps was about 5 arc-sec. The overall accuracy including the optical data was 5-10 arc-sec.

3. OBSERVATIONAL RESULTS

Figure 1 presents the 6 cm maps in total intensity (left) and circular polarization (right) of active region H421 (top) and H419 (bottom), observed on 16 November, 1500 - 1645 UT. The crosses denote the centers of the large sunspots lying within the area of the radio maps. To illustrate the relation of the microwave emission to hot ($T_e > 10^6$ K) coronal loops and to the photospheric magnetic field, we show the radio intensity contours of AR H421 (Figure 2) and AR H419 (Figure 3) superimposed on a soft X-ray image (top) and on a photospheric magnetogram (bottom).

Table I lists the brightest microwave components in each region in approximately decreasing order of brightness temperature (T_b). For each source its estimated size, dominant polarity and degree of polarization (V/I), and possible physical association are also listed. For each active region the source components are indicated on the intensity maps in Figure 1. It should be emphasized that we studied only the <u>brightest</u> microwave components in these regions. The VLA configuration used was not sensitive to large structures or low brightness sources (e.g., plages), but was optimal for observation of the compact, bright coronal

structures typical of ARs. The noise level of the maps was about T_b = 4 x 10^5 K. We concluded that the X-ray and microwave sources in these two regions were quiescent, i.e. that no obvious flares or bursts occurred there during the period of observation. The limitations of this statement are discussed in the final section.

3.1 Active Region H421

Active region H421 was closer to disk center than H419 (r ~ 0.75 from sun center) on 16 November and therefore suffered less from projection effects and off-axis vignetting and scattering in X-rays. It was apparently evolving rapidly, because BBSO observations on 18 November showed a dramatic change in the region with considerable emerging flux in the area to the northwest of the main spot. Region H421 contained one dominant sunspot with penumbra of negative polarity and many small spots or pores. The large spot had an area of 50 millionths of a solar hemisphere and a field strength $\lesssim$ 2000 G (Solar Geophysical Data, 1980).

The bright coronal X-ray structure of AR H421 consisted of two loop arcades crossing the N-S magnetic inversion lines of the region. The arcades were potential-like, with their loops oriented orthogonally to the inversion line. The salient X-ray feature was a short, bright loop (arrow, Figure 2a) which bridged the inversion line in an area of high field gradient near the spot. The western foot of the loop ended at the edge of the spot penumbra. The length (~ 2 x 10^4 km), shape and location of this loop are typical of a class of X-ray loops called penumbral loops (Webb and Zirin, 1981). The inversion line swung in toward the spot and was marked by a short H_α filament; the bright loop appeared to cross over this structure at a small angle, indicative of a high degree of shear in the coronal magnetic field. The bright loop and the eastern

arcade crossed the area of the highest field gradients in the region.

In order to determine parameters of the coronal magnetic field, it is important to identify components of the bright X-ray loop in the microwave map (e.g., Kundu et al., 1980). Unfortunately, the 6 cm components in this region were tightly clustered precluding an unambiguous identification. The component 421E appeared to be coincident with the eastern foot of the loop, and the weak component E' to the west with the top of the loop. But component E, left circularly polarized (LCP), also appeared to straddle the photospheric inversion line. If E was at the loop footpoint, then it lay east of the inversion line but was of reversed polarity to the photospheric field. Alternatively E might have marked the location of a neutral sheet or arcades crossing the inversion line.

The brightest microwave components in AR H421 were < 2 to 7 arc-sec in diameter. Components A, B, C and D lay south of the eastern X-ray arcade and well east of the inversion line (Figure 2). The photospheric field, especially underlying A, was strong and of positive polarity. Although the central polarization of this group was LCP, it was surrounded by islands of RCP indicating the bipolar nature of the group (Figure 1b). The component A, which had the brightest peak (T_b = 10.5 x 10^6 K) observed in either active region, was of LCP, weakly polarized (~ 20%) and was coincident with an Hα patch which later brightened and with several pores. Just north of A was a region of strong RCP (A'). This suggests that A and A' were at the feet of an arcade of short loops. The proximity of the pores and the H_α brightening suggests that strong emission around A might have been associated with neutral sheets in the corona over emerging flux (Kundu and Velusamy, 1980). The

optical coverage was not adequate to definitely identify such emerging flux.

There were no obvious features underlying components B and C in the southern part of this group. C was flanked by two compact sources of RCP (C' in Figure 1b) suggesting bipolarity. All of the brightest sources in H421 had lower circular polarization (20-30%) except for D which was highly polarized ($\gtrsim$ 60%).

An inclusion of negative photospheric polarity east of the neutral line (arrow, Figure 2c) was adjacent to an area of Hα brightening and faint X-ray and microwave emission, but the alignment accuracy precluded a definite association.

The components I, J and K straddled a large, quiescent filament which ran generally E-W and bounded the active region to the south. Since large coronal arcades are known to overlie filaments and filament channels (McIntosh et al., 1976; Webb and Zirin, 1981), the radio sources I and K probably were emission from the legs or feet of loops crossing the filament. Component I', the southern extension of I, overlay the filament; its emission probably came from the top of an arcade loop. The opposite polarization of the components J and F indicates that they outlined compact loop structures crossing a second inversion line north of the filament. The proximity of these two inversion lines suggests that this area was magnetically complex with high field gradients.

North of the sunspot was a classic arcade structure with X-ray loops joining opposite polarity plage divided by a faint filament. The brightest X-ray structure was a large, diffuse arch defining the northern limit of the arcade. Superimposed near the top of this arch was

component H, a bipolar source with peak $T_b \sim 2.5 \times 10^6$ K. The component was of predominantly RCP.

Finally, the component G was compact, bright and entirely of RCP. It was ~ 25 arc-sec west of the center of the spot in an area of mixed photospheric polarity. It could have been associated with the penumbral field, especially since there were no bright X-ray or H_α structures in the vicinity.

3.2 Active Region H419

Region H419 was 2-3 rotations old and appeared stable. However, it was magnetically more complex than region H421 with a dominant preceding spot with a large penumbra and some pores, and two trailing spots. The large p spot, numbered R21 by Mt. Wilson, had an area of 270 millionths and a field strength of ~ 2500 G. The smaller central negative spot, V17/20, and the trailing positive spot, R20, were of nearly equal size. Two of the sunspots (R21 and V17/20) lay within the field of the radio map (Figures 1 and 3). The large leading spot had many, bright microwave components clustered nearby.

The AR was characterized by diffuse X-ray emission spreading linearly in an E - W band. The most notable X-ray feature was a bright, compact structure, which was not associated with 6 cm emission, on the perimeter of the central spot penumbra. Several bright loops to the west were just outside of the field of view of the radio observations. Within this field of view the coronal emission generally bridged inversion lines.

We first discuss the microwave components surrounding the leader sunspot. Figure 4a shows details of the spot structure as seen in the continuum at 1935 UT. A small spot lay within the southeast border of

the penumbra, and several pores lay just outside the penumbra. The BBSO film revealed no appreciable changes in the leader sunspot and the pores around it between about 1600 UT, when the radio and X-ray data were obtained, and 1935 UT.

Figure 4b shows the microwave components superimposed over the same continuum image. This comparison illustrates the following points: 1) The brightest components (A, B, C and H with T_b = 4-7.2 x 10^6 K) were clustered in the vicinity of the penumbral spot and pores about 20-25 arc-sec south of the umbral center; the spots and pores were all of the same polarity; 2) The strongest components (A, B and C) were all LCP or of reversed polarity to the photosphere; 3) The small penumbral spot was associated with a region of low T_b, i.e., a "hole" surrounded by bright emission. The components A, B and C were in areas devoid of significant H_α or X-ray emission. Their higher T_b, lower polarization (20-50%), and association with the high field strengths and gradients of the penumbra and pores suggest that this emission was due to a gyromagnetic mechanism.

About 30 arc-sec south of the sunspot umbra was a bright V-shaped area of X-ray emission associated with H_α fibrils. The multiple, elongated radio components J overlay this area. The N-S orientation of this microwave pattern, the X-ray structure, and the H_α fibrils suggest that the emission arose from an arcade of low-lying loops crossing the inversion line.

The central sunspot in AR H419 (Figure 4a) like the spot in AR H421, had a well developed penumbra with no X-ray or microwave emission above it. The nearest radio components were D and G, 15-20 arc-sec away, at the perimeter of the penumbra.

The area surrounding this spot was the scene of significant activity in the visible in the H_α film. The brightest X-ray feature coincided with a negative magnetic spot in a moat of positive flux at the northern edge of the penumbra (top arrow; Figure 3c). Of flare-like brightness in H_α from 1650 to 1720 UT, this area was active all day and reminiscent of the hot transient penumbral spots studied by Webb and Zirin (1981). This spot was not bright in microwaves, a point we will discuss later. A pore (arrow; Figure 4a) adjacent to the location of the magnetic knot emerged after our observing period.

The small positive polarity arc visible south of the sunspot (bottom arrow; Figure 3c) represents an inclusion of opposite polarity in the general field of the spot. It coincided with dark H_α fibrils emanating from the edge of the spot and was located between the microwave components D and N. The arc was more likely associated with N because this component was RCP, of the same polarity as the magnetic arc, and projection effects would have shifted it to the northwest.

The component D was a bright ($T_b \sim 5 \times 10^6$ K), compact source which lay just south of the sunspot penumbra. It was highly polarized (83%) in LCP, the same sense as the nearby spot polarity. Component G was a double source which overlay the penumbra. Both components D and G were likely associated with penumbral loops.

The chain of components labelled E in Figure 1c overlay an area of negative polarity to the east and positive polarity to the west, an area of high field gradients. The component F was bright and overlay a patch of H_α emission, but was weakly polarized or unpolarized. This suggests emission from the top of a loop.

Three fainter components, M, P and Q, appeared to be associated

with X-ray loops. The large component M coincided with the top of a long, narrow X-ray loop, in a manner similar to that of component H in AR H421. The X-ray loop may have been evolving since its feet were brighter than its midsection (Figure 3a); most quiescent X-ray loops are isobaric.

4. SUMMARY

The key results of our comparative study for 16 November 1979 are:

1) The association between the microwave components and coronal X-ray structures is complex. In general X-ray emitting structures were not associated with the microwave components. This result is supported by Schmahl, et al. (1982).

2) The association between the microwave components and photospheric magnetic fields is likewise complex. Although about half of the radio components were associated with strong photospheric fields, such strong fields did not always produce centimetric emission. The brightest microwave components were associated with areas of strong longitudinal magnetic fields or high field gradients, but not with sunspot umbrae.

3) About one-third of the sources appeared to be associated with only the feet or legs of coronal loops of size $\lesssim 5 \times 10^4$ km. However, only some of these loops were observed in X-rays. The existence of others was deduced from the geometry of the surrounding magnetic field.

4) There were five cases of possible microwave emission from the tops of coronal loops (Table II). Four of these loops, or loop arcades were identified by their emission in X-rays. These components were fainter ($T_b \lesssim 2.5 \times 10^6$ K) and more diffuse than the other components, but had one dominant polarization.

5) None of the sunspot umbrae studied had overlying X-ray emission; i.e., there is little if any material at coronal temperatures over spots. This agrees with previous coronal observation (Pallavicini et al., 1979; Webb and Zirin, 1981; Webb, 1981; Nicholas et al., 1981). Two of the 3 sunspot umbrae and the largest pore for which we had radio observations had no significant microwave emission over them. This result is also supported by other recent measurements at high spatial resolution (Kundu and Velusamy, 1980; Kundu, et al., 1981; Pallavicini et al., 1981). The one sunspot with associated microwave emission (component 419I) was also the largest in both area and magnetic field strength. This observation is consistent with the recent model of Pallavicini et al. (1981), which shows that thermal g-r emission may arise only over umbrae of sufficiently large size.

6) Finally, the sense of 6 cm circular polarization was often reversed with respect to the underlying photospheric field, especially for the bright components. Also, in nearly every case where we interpreted the centimetric components as denoting the legs or feet of loops, one or both components had reversed polarization. We believe that these reversals are related to mode coupling in a quasi-transverse region (Kundu et al., 1977; Bandeira, 1982).

5. DISCUSSION

A major result of this study is that a majority of the individual bright microwave components we identified were not associated with sunspots. This result is contrary to the low resolution radio observations, i.e., that the centimetric core emission from ARs is only associated with spot umbrae. To quantify our assertion we drew circles with

diameters equal to the largest measured diameters of the penumbra and centered on the umbra of each of the 3 spots we observed. In addition we drew concentric circles 10 arc-sec in diameter larger to allow for alignment uncertainties. Sources which lay within or touched these circles were defined to be "associated" with the sunspot. Thirty-two components for both ARs are listed in Table I. Of these only seven lay within the three inner circles and a total of 13 lay within the three outer circles. Therefore, 19, or 59% of the components were definitely not associated with sunspots using our criteria. This number is conservative because we did not correct for penumbral foreshortening and we grouped similarly structured sources together (e.g., 419E).

The existence of such a large number of strong components, not all associated with regions of strong photospheric magnetic field, and with a low correlation with X-ray structures means that mechanisms invoked to explain the radio sources must apply over a large range of magnetic field strengths and outside of the range of plasma parameters typical of ARs.

We can use the X-ray observations to constrain these emission mechanisms. First, although low brightness temperatures suggestive of thermal bremsstrahlung may be typical of the extended, plage-associated component of active regions (Kundu et al., 1977; Pallavicini et al., 1981; Felli et al., 1981), we can rule out bremsstrahlung as a significant contributor to the bright radio emission studied here. Most of the material in a typical active region is at coronal temperatures ($T_e > 10^6$ K), and is visible in broadband X-rays (see Webb, 1981 for a review). Therefore, since the corona is optically thin to bremsstrahlung in both broadband X-rays and at 6 cm, we can estimate the contribution

of bremsstrahlung to the observed brightness temperature, T_b, of those centimetric components associated with X-ray structures. The 4 components associated with the X-ray loops (Table II) have brightness temperatures consistent with their being optically thin to bremsstrahlung (quiescent X-ray loops invariably have T_e = 2-3 x 10^6 K). In the optically thin case the predicted T_b is:

$$T_b = \frac{\xi}{\nu^2 T_e^{1/2}} \int n_e^2 \, dl$$

where $\int n_e^2$ dl is the thermal emission measure along the line of sight derived from X-ray observations, ν is the frequency of the radio observations, and ξ has a value of 0.16 in the corona (Kundu, 1965). Using an appropriate value for n_e^2 dl in X-ray loops of $\sim 10^{28}$ cm^{-5}, $T_b \sim 5 \times 10^4$ K at 5 GHz, too low a value to explain the bright radio emission.

Gyromagnetic emission mechanisms provide the only known alternative explanation to bremsstrahlung for the bright components of the slowly varying radiation. Nonthermal gyrosynchroton processes have been invoked, but these require continuous acceleration of electrons to explain the long lifetime of the bright components and more polarization diversity than observed. The fact that the radio brightness temperatures and the coronal electron temperatures are often nearly equal argues for a thermal mechanism (e.g., Kundu et al., 1980), such as resonance absorption at harmonics of the gyrofrequency.

This theory predicts that in coronal loops, which should be optically thin to bremsstrahlung, the gyroresonance (g-r) absorption process makes the radio emission optically thick where the magnetic field strength is high and where the angle Θ between the magnetic field

direction and the line of sight is large (Kundu et al., 1977; Gel'freikh and Lubyshev, 1979). This mechanism has been invoked in an interpretation of bright non-sunspot components in terms of neutral sheets overlying emerging flux (Kundu and Velusamy, 1980), or emission from the tops of loops bridging magnetic inversion lines (e.g., Kundu et al., 1977). In support of these interpretations, we find that generally the microwave components we observed were in regions where strong magnetic fields or high field gradients might be expected.

Figure 5 is a plot of the resonant optically thick layers as a function of temperature and electron density from the g-r theory. The curved lines indicate the limiting sensitivity of the AS&E X-ray rocket experiment for the detection of coronal loops at two fixed diameters, the maximum diameter (left) of typical AR X-ray loops and the average diameter (right) of loops in one well-studied AR (Pye et al, 1978). Structures which lie to the left of these curves in terms of their electron temperature and density could not be detected in X-rays. Figure 5 implies that for those components lacking significant X-ray emission, resonance emission can only occur at the second harmonic or at high values of θ at the third harmonic. Six cm emission at these harmonics requires fields of 900 and 600 G, respectively, in the corona. But about half of the components overlie regions where the photospheric magnetic field is less than these values. Even for those components with possible, faint X-ray emission (e.g., 421 F) it is very unlikely that harmonics higher than 3 (and therefore lower field strengths) can be responsible for the g-r emission. Therefore, for many of the microwave components, the g-r theory implies unreasonably high magnetic field strengths in the corona.

A different problem arises in interpreting the emission from the brightest ($T_b > 4 \times 10^6$ K) components in each region. Most of these components were associated with reasonably strong photospheric magnetic fields, but not with X-ray emission or sunspot umbrae. For a thermal interpretation of the radio emission, $T_b \leq T_e$. Therefore, a g-r explanation demands very high electron temperatures, low densities ($< 10^8$ cm^{-3}) and high coronal field strengths. We speculate on two possible explanations for this emission. High field strengths could be produced in coronal loops with significant currents. But it is difficult to understand why such currents would not also heat the loops sufficiently to emit in X-rays unless they have very low density. Hollweg (1981) recently reviewed mechanisms for producing nonthermal radio emission from runaway electrons in the corona. But "hot" loops, which were not observed here, and high electric fields are requirements for such coronal radio emission. It is possible that such large electric fields are produced in the transition region, where the large temperature gradient and strong magnetic fields can readily accelerate electrons (J. Ionson, private communication). If such an interpretation for the bright, non-sunspot microwave sources is correct, then our observation of numerous, nonvarying bright sources in two undistinguished ARs suggests that continuous acceleration of particles may be common in ARs.

It is possible that we failed to detect small-scale transient or burst activity in these sources. We did not observe such activity within the limitations of our study. For instance, no H_α flares were reported in the Solar Geophysical Data bulletins in either region on 16 November nor were any detected in H419 on the BBSO film. There were no significant fluctuations observed in soft X-rays between 1000 and 2030

UT by the NOAA/GOES satellite at 1-8 Å. There were no changes observed on the six KPNO magnetograms obtained between 1543 and 2100 UT. Finally, no statistically significant time variations in the integrated microwave flux were observed during continuous scanning from 1500-1645 UT. However, we can not rule out the possibility of some significant variability in one or more of the bright components. In addition, the spectral characteristics of the radiation useful in distinguishing thermal and nonthermal contributions were unknown.

We find that the presence of strong, longitudinal magnetic fields is not a sufficient condition for bright microwave emission. Although many of the brightest microwave components were associated with regions of strong photospheric fields, there were other regions of apparently strong field that had no bright emission. For example, in AR H421 single pores and clusters of pores north of the main sunspot had no associated microwave emission. Also, the presence of an isolated magnetic knot north of the central sunspot of AR H419 was cospatial with bright, flarelike patches in H_α and X-rays, but was void of microwave emission. The dependence of g-r emission on the geometry of the magnetic field and the plasma distribution apparently restricts this emission to only a limited number of coronal structures with high magnetic fields.

If the microwave emission at T_b = 1-4 x 10^6 K is due primarily to the g-r process, we can understand the lack of association between the X-ray emitting structures and the bright centimetric components. High g-r opacity is a function of a strong magnetic field and the angle θ. If the field is too weak, the resonance layer will not be optically thick and no emission will be observed. Since X-ray emitting plasma is confined by the magnetic field in loops and the corona is highly

conducting, the internal loop field strength should be low. For instance, the equipartition field strength in typical AR loops is only a few gauss and potential field extrapolations yield values of a few to tens of gauss in some AR loops (e.g., Poletto et al., 1975; Levine and Withbroe, 1977). Although X-ray emission certainly arises from some loops associated with strong field regions (e.g., Webb and Zirin, 1981), most quiescent AR X-ray loops do not terminate in such regions. Therefore, we should not necessarily expect bright centimeter emission from typical AR X-ray loops.

ACKNOWLEDGEMENTS

The authors are grateful to the following individuals for participating in and providing data for the observations discussed in this paper: J. Harvey of KPNO for the magnetograms, H. Zirin and A. Patterson of BBSO for the optical filtergrams, R. Howard of the Mt. Wilson Observatory for sunspot positions, and P. McIntosh of the NOAA Space Environment Laboratory for an H_α image. We thank S. Bichisecchi of the AS&E photographic laboratory for his assistance with the imagery used in this study. We benefited from discussions with E. Schmahl, S. Kahler and A. Krieger. DFW and JMD were supported at AS&E by NASA Contract NAS5-25496. MRK and TV were supported at the University of Maryland by NSF Grant ATM 81-030839, NASA Grant NGR 21-002-199, and NASA Contract NSG 5320.

TABLE I

Source	Peak T_b (10^6 K)	Size[a] (arc sec)	Peak Polarity[b]	Reversed?[c]	Polarization (%)[d]	Association
421 A	10.5	7 x 9	L	R	23	Photospheric pores - emerging flux loops
421 B	8	7 x 5	L	R	∿30	Foot of bright loop?
421 C	6.5	6 x 6	L	R	30	?
421 D	6.5	< 2	L	R	62	?
421 E	4.8	4 x 5	L	?	33	Foot of bright loop?
421 E'	1.5	4 x 5	L	S	--	Top of bright loop
421 F	3.2	3 x 11	L	R	25	Foot of bright loop or of arcade loop
421 G	3.2	5 x 5	R	?	25	Penumbra or neutral line
421 H	2.5	8 x 6	R	S?	33	Top of coronal arcade
421 I	1.5	3 x 9	L	R?	100	Foot of filament arcade loop
421 I'	1.5	3 x 12	L	--	--	Top of filament arcade loop.
421 J	1.5	3 x 4	R	?	50	Foot of arcade loops.
421 K	1.5	3 x 5	R?	R?	--	Foot of filament arcade loop
421 L	∿1	diffuse	R	R	--	Small loop over magnetic cell
419 A	7.2	7 x 5	L	R	22	Photospheric pore and/or penumbra
419 B	6.5	11 x 6	L	R	50	Photospheric pore and/or penumbra
419 C	4.8	2 x 3	L	R	40	Photospheric pore and/or Penumbra

419 D	4.8	12 x 6	L	S	83	Penumbral loops
419 E	1.5 - 4.8	15 x 7	R	S and R	40-100	Neutral line with high field gradients
419 F	4	7 x 4	L?	S?	?	Top of loop?
419 G	4	12 x 5	L	S	80	Penumbral loops
419 H	4	6 x 4	R	S	60-80	Photospheric pore and/or penumbra
419 I	3.2	4 x 5	R	S?	50	Sunspot umbra
419 J	1.5 - 2.5	15 x 8	R	S	33-100	Loop arcade crossing NL
419 K	2.5	5 x 3	R	S	33	?
419 L	1.5	10 x 3	R	?	50	?
419 M	1.5	12 x 6	R	?	50	Top of long X-ray loop
419 N	1.5	6 x 3	R	S or R	--	Magnetic cell or foot of penumbral loops
419 O	∿1	diffuse	L	?	--	Foot of loops
419 P	1.5	6 x 5	L	?	100	Foot of X-ray loop?
419 Q	2.5	9 x 5	L	R?	100	Foot of X-ray loop ?
419 R	1.5	diffuse	L	?	?	Foot of filament arcade loop?

a = The approximate FWHM dimensions of the total intensity along the short and long axis of each component. These have not been corrected for the beam shape.

b = The sense of circular polarization at the peak intensity of the component. L is left CP (negative) and R is right CP (positive).

c = Whether the sense of circular polarization (b) is the same (S) or reversed (R) with respect to the underlying photospheric magnetic field. This assignment does not account for projection effects.

d = Degree of polarization %(V/I) at the peak intensity of the component.

TABLE II

SOURCES AT TOPS OF CORONAL LOOPS

Source	Peak T_b (10^6K)	Peak Polarity	X-Radiation	Association
421 E'	1.5	L	yes	Bright penumbral loop.
421 H	2.5	R	yes	Bright loop arcade over neutral line.
419 J	1.5-2.5	R	yes	Loop arcade over neutral line.
419 M	1.5	R	yes	Long single loop.
421 I'	1.5	L	no	Possible filament arcade loop.

REFERENCES

Alissandrakis, C.E., Kundu, M.R. and Lantos, P.: 1980, Astron. and Astrophys. 82, 30.

Bandeira, R.: 1982, Astron. and Astrophys. 112, 52.

Davis, J.M., Krieger, A.S., Silk, J.K. and Chase, R.C.: 1979, SPIE 184, 96.

Felli, M., Lang, K.R. and Willson, R.F.: 1981, Astrophys. J. 247, 325.

Gel'freikh, G.B. and Lubyshev, B.I.: 1979, Soviet Astron. 23, 316.

Gerassimenko, M., Nolte, J.T. and Petrasso, R.D.: 1976, Solar Phys. 48, 121.

Hollweg, J.V.: 1981, in F.Q. Orrall (ed.) Solar Active Regions, Colorado Associated University Press, Boulder, CO.

Kundu, M.R.: 1965, Solar Radio Astronomy, Interscience, New York.

Kundu, M.R. and Velusamy, T.: 1980, Astrophys. J. 240, L63.

Kundu, M.R., Alissandrakis, C.E., Bregman, J.D., and Hin, A.C.: 1977, Astrophys. J. 213, 278.

Kundu, M.R., Schmahl, E.J. and Gerassimenko, M.: 1980, Astron. and Astrophys. 82, 265.

Kundu, M.R., Schmahl, E.J. and Rao, A.P.: 1981, Astron. Astrophys. 94, 72.

Levine, R.H. and Withbroe, G.L.: 1977, Solar Phys. 51, 83.

McIntosh, P.S., Krieger, A.S., Nolte, J.T. and Vaiana, G.: 1976, Solar

Phys. 49, 57.

Nicholas, K.R., Kjeldseth-Moe, O., Bartoe, J.-D. and Brueckner, G.E.: 1981, Solar Phys. (submitted).

Pallavicini, R., Sakurai, T. and Vaiana, G.S.: 1981, Astron. Astrophys. 98, 316.

Pallavicini, R., Vaiana, G.S., Tofani, G. and Felli, M.: 1979, Astrophys. J. 229, 375.

Poletto, G., Vaiana, G.S., Zombeck, M.V., Krieger, A.S. and Timothy, A.F.: 1975, Solar Phys. 44, 83.

Pye, J.P., Evans, K.D., Hutcheon, R.J., Gerassimenko, M., Davis, J.M., Krieger, A.S. and Vesecky, J.F.: 1978, Astron. Astrophys. 65, 123.

Schmahl, E.J., Kundu, M.R., Strong, K.T., Bentley, R.D., Smith, J.B., Jr. and Krall, K.R.: 1982, Solar Phys. (in press).

Solar Geophysical Data, 1980, U.S. Department of Commerce, NOAA, Boulder, CO.

Vaiana, G.S., Krieger, A.S. and Timothy, A.F.: 1973, Solar Phys. 32, 81.

Webb, D.F.: 1981, in F.Q. Orrall (ed.) Solar Active Regions, Colorado Associated University Press, Boulder, CO.

Webb, D.F. and Zirin, H.: 1981, Solar Phys. 69, 99.

FIGURE CAPTIONS

Figure 1. 6 cm VLA maps of active regions H16421 (top) and H16419 (bottom) on 16 November 1979. The size of the synthesized beam was 6 x 3 arc-sec. Geocentric north is at the top and east to the left. The center (0,0) of the H16421 map was at 263 arc-sec north and 316 arc-sec west of disk center at 1600 UT, and the center (0,0) of the H16419 map was at 660 arc-sec north and 342 arc-sec west of disk center. (a) Total intensity (R+L) map of H16421. The lowest contour and the contour interval is 8 x 10^5 K. The cross shows the centroid of the large sunspot V15/17 in Mt. Wilson group no. 21042; the length of the arms of the cross is 10 arc-sec, which is representative of the alignment uncertainties. The letters designate individual microwave components. (b) Circularly polarized (R-L) intensity map of H16421. The first two contours are 4 and 8 x 10^5 K, respectively, and the contour interval for the higher contours is 8 x 10^5 K. The solid (broken) contours represent positive (negative) values. (c) Total intensity map of H16419. The contour levels are the same as (a). The crosses show the centroids of sunspots V17/20 and R21 in the Mt. Wilson group no. 21041. (d) Circularly polarized intensity map of H16419. The contour levels are the same as (b).

Figure 2. Coaligned, high resolution images in soft X-rays (top), of the photospheric magnetic field (bottom) and at 6 cm of

active region H16421 on 16 November 1979. The X-ray image is a 60 sec exposure on Kodak SO-253 emulsion. The 6 cm total intensity map from Figure 1a is superimposed on the X-ray and magnetogram images (b and d, respectively), which are shown separately on the left side for clarity. The direction arrows at the bottom denote heliographic directions.

Figure 3. Coaligned images similar to Figure 2 for active region H16419 on 16 November 1979.

Figure 4. (a) Near-H_α continuum image of AR H16419 at 1935 UT on 16 November 1979 showing the sunspot structure. The arrow points to a pore that appeared after 1700 UT. (b) The same image with the 6 cm total intensity map of Figure 1c superimposed on it.

Figure 5. Loop temperatures and electron densities required to reach unit optical depth at resonant harmonics, s, of the gyrofrequency. The observing frequency is 5 GHz and the scale length of the magnetic field strength is assumed to be 10^9 cm. The optical depth is larger (smaller) than unity on the right (left) side of each curve. The curved lines represent the limiting sensitivity to X-ray structures and are discussed in the text. (After Kundu et al., 1980, Figure 2.)

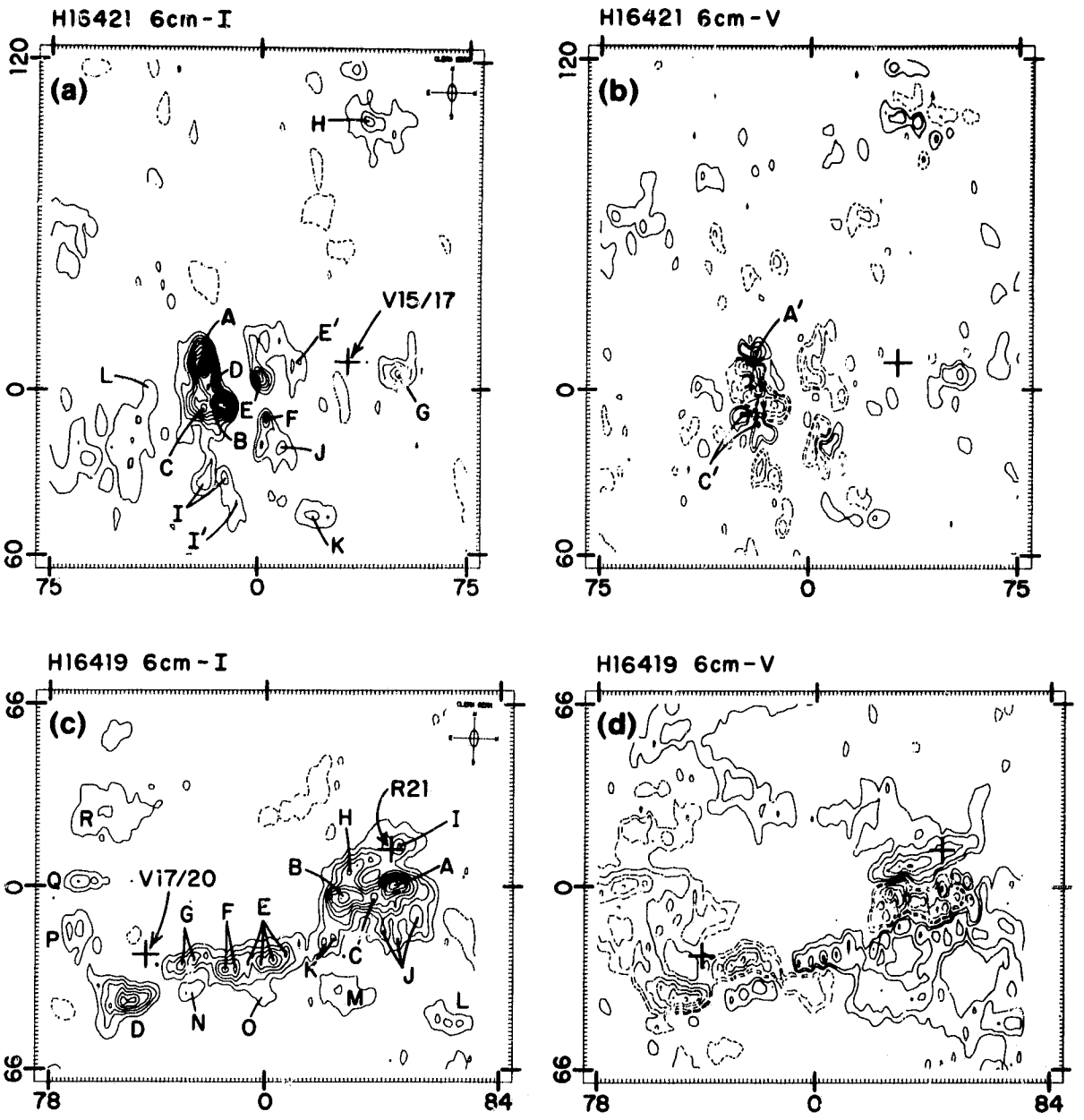

Figure - 1

H 421

a) X-RAY. 1704 UT

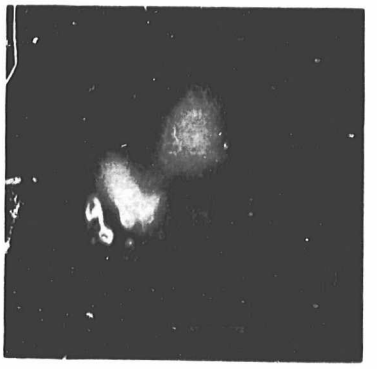

b) X-RAY + 6 CM

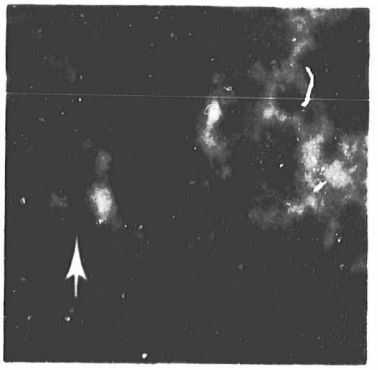

c) MAG: 1742 UT

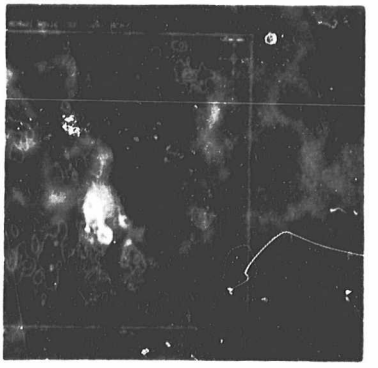

d) MAG + 6 CM

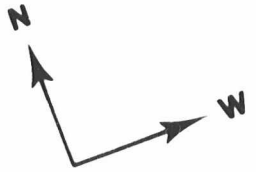

Figure - 2

H 419

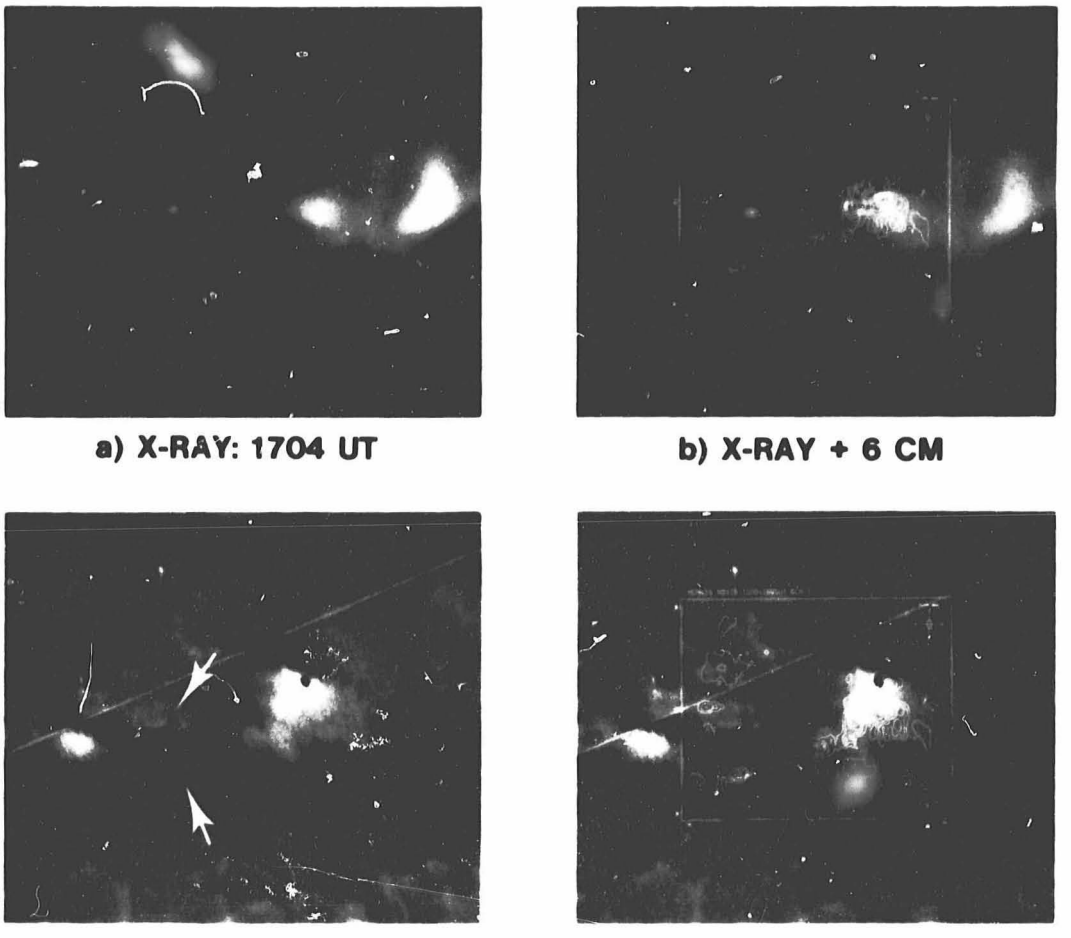

Figure - 3

H 419

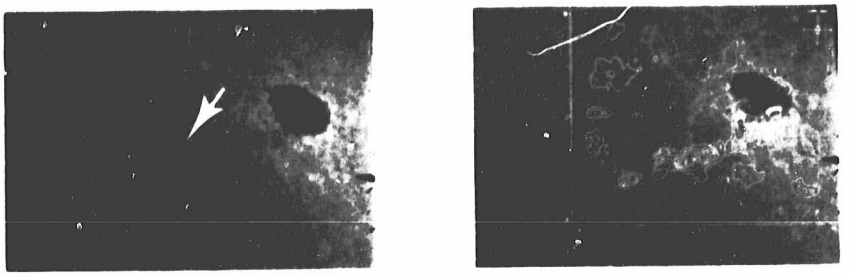

a. b.

Figure - 4

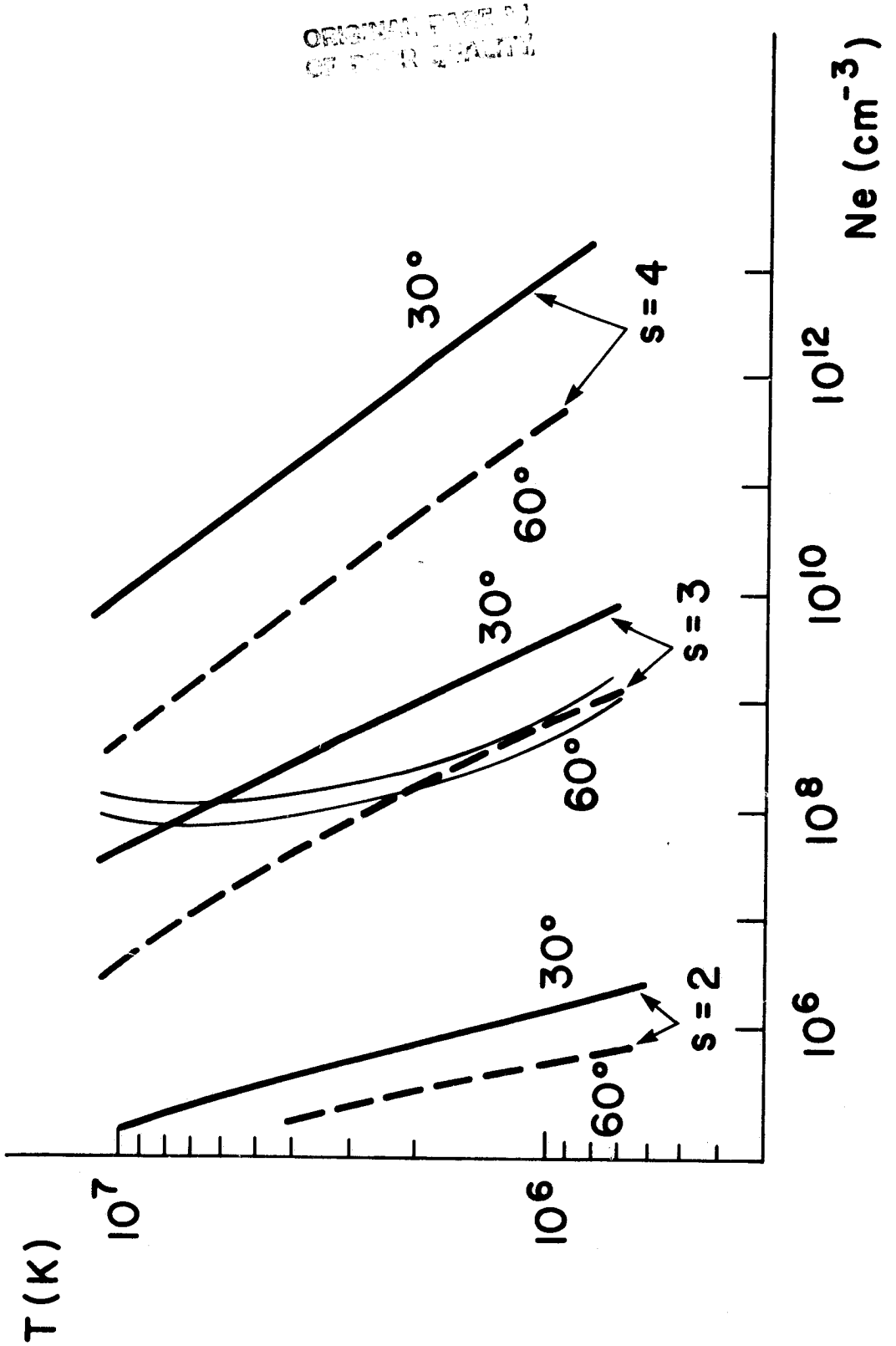

Figure - 5

4.2 Comparison of Coronal Holes Observed in Soft X-ray and HeI-10830ÅSpectroheliograms

S.W. Kahler and J.M. Davis

American Science and Engineering, Inc.
Cambridge, Mass.

and

J.W. Harvey

Kitt Peak National Observatory
Tucson, Arizona

ASE-4761

COMPARISON OF CORONAL HOLES OBSERVED IN SOFT X-RAY AND HE I 10830 Å SPECTROHELIOGRAMS

by S.W. Kahler and J.M. Davis

American Science and Engineering, Inc.
Fort Washington
Cambridge, MA 02139, U.S.A

and

J.W. Harvey

Kitt Peak National Observatory*
Tucson, AZ 85726, U.S.A

Accepted for Publication in SOLAR PHYSICS, March 1983

* Operated by the Association of Universities for Research in Astronomy, Inc., under contract with the National Science Foundation.

ABSTRACT

We compare coronal holes observed in solar soft X-ray images obtained with rocket-borne telescopes during 1974 to 1981 with holes observed on nearly simultaneous 10830 Å maps. Hole boundaries are frequently poorly defined, and after 1974 the brightness contrast between the large scale structure and holes appears substantially diminished in both X-rays and 10830 Å. We find good agreement between soft X-rays and 10830 Å for large area holes but poor agreement for mid and low latitude small area holes, which are generally of low contrast. These results appear inconsistent with the popular view that the quiet corona is sharply separated into open magnetic field regions consisting of coronal holes and closed field regions consisting of the large scale structure.

1. INTRODUCTION

Coronal hole research was greatly stimulated by the solar soft X-ray and XUV observations during the Skylab mission in 1973-1974. High resolution images showing coronal holes devoid of coronal emission were available on at least a daily basis and over many solar rotations. The holes were found to be regions of magnetic field open to the interplanetary medium and inferred to be the sources of high speed wind streams. The Skylab results of coronal hole studies were summarized by Zirker (1977).

The end of the Skylab mission stimulated a search for alternative sources of information to identify coronal holes. During the mission a number of full disk spectroheliograms were obtained at Kitt Peak National Observatory in the D_3 line of He I at 5876 Å. A qualitative comparison by Harvey et al. (1974) of the KPNO D_3 spectroheliograms with the American Science and Engineering soft X-ray images from Skylab showed promising results for detecting coronal holes in the D_3 line. Improved signal-to-noise ratio observations, using the He I 10830 Å, became possible at KPNO by the end of the Skylab mission. One such observation was compared with a Skylab He II 304 Å observation by Harvey and Sheeley (1977) and confirmed that a coronal hole was indeed detectable with 10830 Å. However, because routine 10830 Å observations were started just after the Skylab mission, no direct comparisons between the 10830 Å and Skylab soft X-ray data could be made.

The contrast between coronal holes and the quiet corona viewed in the 10830 A line is due to the enhanced population in the quiet corona of the triplet state of He I, which absorbs the continuum radiation from below. The physical problem posed by the observations is why the excited 1s2s ground state of the 10830 Å transition should be so abundant when it is 19.7 electron volts above the ground state in an ion formed at chromospheric temperatures. Helium is unique in this respect since coronal holes cannot be discerned in lines of other abundant elements formed at chromospheric or transition region temperatures (Huber et al., 1974). Goldberg (1939) suggested that an excess of ultraviolet radiation in the 500 Å region could ionize He I from its ground state. This enhanced ionization mechanism, together with the metastability of the 1s2s triplet state, would thus explain the depleted population of singlet levels.

Zirin (1975) found that calculations of a model in which He is photoionized by coronal radiation and then recombines to populate the upper states were in good agreement with line intensity observations. He dismissed attempts to explain the He lines with collisional excitation models, specifically that of Milkey et al. (1973), as hopeless. His model as the dominant process for He line formation was soon attacked by Milkey (1975) on the grounds of an incompatibility with the observed line profiles. Shortly afterwards, Shine et al. (1975) developed a model of thermal diffusion of He ions into the transition region resulting in an enhanced rate of excitational collisions with high temperature electrons. Although Skylab XUV observations of the center-to-limb variations of He lines by Mango et al. (1978) and Glacken et al. (1978) suggested collisional excitation of the He I 1s2s triplet state, the question of the primary excitation process still remains unsettled.

For our purposes the important fact is that the presence of the triplet state and consequent 10830 Å absorption in the chromosphere is closely coupled to the presence of overlying hot coronal material. Because of this, the distinction between active regions and the quiet corona is sharp in the 10830 Å images as it is in X-ray images. However, the correspondence between X-ray coronal holes and holes inferred from the 10830 Å maps has been examined only for the 27 June 1974 X-ray image obtained with an AS&E rocket observation (Harvey and Sheeley, 1979). In that case only one large hole near central meridian was seen, and no detailed comparisons of the 10830 Å and X-ray hole boundaries was made. Since the 10830 Å images are now widely used to infer coronal holes (Sheeley and Harvey, 1981), it is appropriate to compare in detail the coronal holes observed in the X-ray images obtained in the AS&E solar rocket program with those of the corresponding KPNO 10830 Å images.

2. DATA ANALYSIS

2.1 Instrumentation

Since the Skylab period the X-ray Sun has been observed with AS&E grazing incidence telescopes on seven rocket flights. On each flight full disk solar X-ray images were recorded on Kodak SO-212 film using a combination of filters and exposure times. During this time daily He I 10830 Å spectroheliograms have been recorded continually at KPNO, except for some coverage gaps ranging from several days to several months in extent. A large coverage gap occurred at the time of the 17 November 1976 flight, so that observation, described by Nolte et al. (1977), is not used in this analysis. Each 10830 Å observation was taken during a 40 minute period by scanning the Sun in 4 swaths each 512 arc sec wide. Except for 27 June 1974, the scans were made in the solar east-west direction. Times shown in the figures are the midpoints of the observing periods. Details of the observations are presented in Harvey and Sheeley (1977).

The dates and times of the rocket images are listed in Table I. Two sets of paraboloid-hyperboloid mirrors have been used in the X-ray rocket program. The reflecting surfaces of the older mirrors, used primarily in pre-Skylab observations, are layers of a nickel alloy, Kanigen, deposited on beryllium. The details of that telescope were discussed by Vaiana et al. (1968) and Giacconi et al. (1969). The newer mirrors, consisting of fused silica (glass), are compared with the Kanigen mirrors in Table 1 of Davis et al. (1977). The principal differences between the two sets of mirrors are that the glass mirrors are characterized by a factor of 2.6 larger effective collecting area at 44 Å and by a substantially reduced point spread function.

Variations among the rocket images in mirrors, filters, and exposure times preclude the use of a uniform set of X-ray images for this study. For each flight, the exposure duration and filter of the image judged best for showing coronal holes is listed in the fourth column of Table I. Images obtained through the polypropylene (pp) filter during the

Skylab mission (Vaiana et al., 1977) were normally used to study coronal holes. Images were obtained through a similar filter on each rocket flight and are used here except for the two cases shown in Table I where images obtained through an ultra-thin aluminum filter were used. On 7 November 1979 instrumental scattering from a flare at S13 E20 washed out the faint regions in the pp image, while the optimum 16 November 1979 pp image was blurred from a pointing rotation. The wavelength passbands at the 1% transmission levels for the chosen filters are given in the last column of the table.

2.2 Determination of Boundaries

Using transparencies overlaid on 10830 Å full disk prints, one of us (JWH) traced the apparent boundaries of inferred coronal holes. In some cases the low brightness intensity rendered the identification of the hole questionable, and these boundaries are indicated in the figures by dashed lines. In a similar manner one of us (SWK) traced the boundaries of coronal holes on transparencies overlaid on high contrast X-ray transparencies. These boundaries were first drawn to include all possible hole areas. Shaded regions were used to indicate areas where the existence of an X-ray coronal hole was questionable. These shaded regions encompassed both entire small hole candidates and the diffuse boundaries of well established holes. The high contrast of the X-ray features in and around holes allowed the X-ray hole boundaries to be traced in greater detail than those of the 10830 Å maps. Each set of hole boundaries was independently traced on images with 10.8 cm disk diameters before the comparisons were made. It should be appreciated that this determination of the position of holes and hole boundaries in both the X-ray and 10830 Å data is a subjective process. One can anticipate differences in hole boundaries determined by different observers or by the same observer at different times.

For two dates the daily 10830 Å maps were not obtained, and it was necessary to project hole boundaries from adjacent dates forward or backward in time to compare with the X-ray hole boundaries. Boundaries from the 2

February 1978 map were projected back to 31 January 1978, and those of 5 November 1979 and 9 November 1979 were projected forward and backward respectively to 7 November 1979. In each case the Newton-Nunn rotation rates (Allen, 1963) determined the displacements traced with Stonyhurst disks.

The 10830 Å and X-ray images were aligned to within an estimated 10 arc sec by means of the active region features which were bright on the X-ray transparencies and dark on the 10830 Å prints. In the three figures the X-ray and 10830 Å boundaries are superposed for each set of images.

2.3 Detailed Comparisons of Hole Boundaries

Large coronal holes show a general correlation in the X-ray and 10830 Å images. The best case is that of 27 June 1974 shown in Figure 1a. The prominent X-ray hole extends from the north pole to about 25° S in latitude and about 50° in longitude at the equator. The eastern boundaries of the X-ray and 10830 Å holes are in good agreement, but elsewhere the X-ray hole is larger, generally by several heliocentric degrees. A small but distinct neck connecting the polar and equatorial X-ray holes is absent in the 10830 Å image. The brightness contrast between the hole and the background corona is higher in this X-ray image than in the others shown here, but even so, we see that extensive parts of the hole boundaries are indistinct as indicated by shaded areas in Figure 1a.

X-ray and 10830 Å boundaries of the large polar holes observed on 13 February 1981 (Figure 1) and 31 January 1978 and 7 November 1979, shown in Figure 2, also agree well to first order. The best agreement in detail is that of 13 February 1981, but that is the only one of the three dates for which simultaneous X-ray and 10830 Å data exist.

The worst agreement between hole boundaries appears in the mid and low latitude small holes of 13 February 1981 (Figure 1) and 7 November 1979 (Figure 2). In the first case no evidence of the five northern latitude holes appears in the X-ray image. Similarly, there is no X-ray analog of

the negative polarity hole in the southeast, but the east-west 10830 Å holes near the south pole do correspond to regions of decreased X-ray brightness. However, these latter features appear to be empty filament channels (McIntosh et al., 1976), rather than holes, when compared to H_α synoptic maps published in Solar-Geophysical Data.

The 7 November 1979 comparison is compromised by the lack of simultaneous data, but here again, four small 10830 Å holes within 40° of central meridian are not associated with obvious holes in the X-ray image, although they do lie in regions of relatively low emission. In addition, an X-ray hole on the equator at the west limb was not associated with a 10830 Å hole.

To a lesser degree the data of Figure 3 also illustrate the poor correspondence of the mid and low latitude holes. The four such holes observed in 10830 Å on 16 September 1976 are all faint and uncertain, as indicated by the dashed lines, and while they correspond to regions of low X-ray brightness, other regions of the X-ray corona are of comparable or lesser brightness. This X-ray image was obtained near solar minimum and shows a generally faint corona. The 16 November 1979 X-ray image reflects a more active sun, and here again the uncertain 10830 Å hole boundaries correspond only roughly to regions of low X-ray brightness. Only two small, doubtful regions appeared as low latitude X-ray holes in that image. The region of 10830 Å emission elongated in the east-west direction at S40° is a filament channel seen in the H_α synoptic charts of Solar-Geophysical Data.

One might expect to detect polar holes more easily in 10830 Å than in X-rays as a result of the obscuration of X-ray polar holes by adjacent bright coronal features such as loop arcades (McIntosh et al., 1976). This does appear to be the case in the 31 January 1978 north and south polar holes (Figure 2), but in general the X-ray holes appear larger at the poles than do the 10830 Å holes. The best example of this is the 27 June 1974 north polar hole in which the X-ray eastern boundary is substantially farther from the pole than is that of the 10830 Å boundary.

The X-ray polar hole is also substantially larger than the 10830 Å hole in those cases where we consider the hatched (uncertain) area of the X-ray hole. The south pole of 13 February 1981, the north pole of 16 September 1976, and both poles of 7 and 16 November 1979 all illustrate this result.

3. DISCUSSION

The Skylab X-ray images have formed the observational basis for the implicit assumption that coronal hole (CH) boundaries are sharp and well defined. Bohlin (1977) has briefly discussed the displacement of apparent hole boundaries due to foreground coronal emission, and Nolte et al. (1976) pointed out the occasional presence of faintly emitting X-ray regions within or near the hole boundaries which rendered those boundaries uncertain, but otherwise no indication of ambiguity in hole boundaries is found in the literature. In fact, in their quantitative Skylab X-ray study of CH1, Maxson and Vaiana (1977) concluded that the transition from coronal hole to large scale structure is sharp. However, they offered no quantitative definition of "sharp", and both their contour plots of the boundaries and histograms of photographic density in and around hole areas suggest that the uncertainties in hole areas are large fractions of the areas themselves. Thus, past studies provide no support for the usual assumption that coronal hole boundaries are well defined.

The contrast between the X-ray brightness of the large coronal hole and that of the large scale structure in the 27 June 1974 image (Figure 1) appears comparable to that of the Skylab images (cf. Zirker, 1977). This contrast appears considerably diminished in the X-ray images of later dates as shown in the figures. Without a quantitative photometric analysis of the X-ray holes and large-scale structures of these images, a definitive statement about possible brightness changes can not be made. However, this apparent decrease in X-ray contrast is accompanied by a comparable contrast decrease in the 10830 Å data, as indicated by the dashed 10830 Å hole boundaries in the figures. It therefore appears that non-polar holes appearing near solar minimum and during the rise phase of the current cycle are not so clearly discerned from the large scale structure as was the case during the declining phase in 1973-1974. This result, coupled with the observation that the hole boundaries are often diffuse, implies that drawing hole boundaries with either X-ray or 10830 Å data is a far more subjective process than previously believed.

Even with the above caveats, we have found a good correlation between the X-ray and 10830 Å data for the presence of large area coronal holes. In two cases (31 January 1978 and 13 February 1981) the large holes were at the south pole and in the other at the equator (27 June 1974). Since the 10830 Å data allows one to infer holes at the chromospheric level, and intervening coronal emission renders polar holes less visible in X-rays, we might expect that these holes would be larger in the 10830 Å data. Evidence of this effect can be seen in the 31 January 1978 polar hole, but it is not the rule. The dominant X-ray polar hole is distinctly larger than the corresponding 10830 Å hole on 27 June 1974, 7 and 16 November 1979, and 13 February 1981, although in the last three cases the excess X-ray hole areas are uncertain as indicated by hatched areas.

We have found the worst agreement between the X-ray and 10830 Å holes at low and mid latitudes. For the period 1976 to 1981, these holes, generally seen in the 10830 Å data as weak holes, were small in diameter (10-20 solar degrees) and usually did not correspond to obvious X-ray holes. In the cases of 16 November 1979 and 13 February 1981 there are weak holes well away from central meridian, so the poor agreement with X-ray holes could be due to projection effects of foreground coronal material. However, all the 10830 Å maps except that of 27 June 1974 have weak holes near central meridian with poor agreement in X-rays, so this effect is not due to projection problems.

Weak 10830 Å holes were reported by Sheeley and Harvey (1981) and appeared most often in their Bartels display during 1976-1977. They also found that the correlation between coronal holes and solar wind streams established during the Skylab period (cf. Zirker, 1977) degraded since 1976. Some recurrent holes had no observed associated wind streams, and in other cases the recurrent streams had lower peak velocities than those of Skylab. Nolte et al. (1977) had also found similar results using the 1976 rocket X-ray images. The role of the weak holes in the deterioration of the wind stream correlation is unclear. Most of the Sheeley and Harvey recurrent holes, confined to $\pm 40°$ latitude, were well defined, whereas in this study the low and mid latitude holes are mostly weak. On

the other hand, some of the well defined holes of the Sheeley and Harvey study may well correspond to the weak holes of this study.

On the basis of the Skylab X-ray images Maxson and Vaiana (1977) have claimed that the quiet solar corona is sharply separated into two different components - the open magnetic field regions associated with coronal holes and closed field regions associated with the large scale structure. The existence of low contrast holes and indistinct hole boundaries in both the 10830 Å and X-ray images of this study is difficult to understand in the context of this two component description. These results suggest the presence of regions where closed and open field lines may be mixed. Evidence for this more complex picture was presented by Levine et al. (1977) based on a comparison of a harmonic analysis of the solar magnetic field with the Skylab X-ray pictures. They found evidence that the formation of open field regions preceded the occurrence of coronal holes by as much as a solar rotation. They also concluded that closed magnetic fields occupied a significant part of the area of coronal holes. More recently, Levine (1982) has presented examples of apparently open magnetic structures which cannot be identifed unambiguously in He I 10830 Å spectroheliograms. Their results and ours suggest that the magnetic field in the quiet corona is complex in a way that is not yet understood.

ACKNOWLEDGEMENTS

We are pleased to acknowledge many helpful discussions with D.F. Webb and the assistance of M. Rizza in the preparation of the photographic evidence. Support for the study at AS&E was provided by NASA under contracts NASW-3586 and NAS5-25496.

TABLE I. ROCKET X-RAY IMAGES

Date	Time (U.T.)	Mirror	Exposure and Filter[a]	Wavelength (Å)
27 June 1974	1948	glass	59 s pp	8-39, 44-64
16 Sept 1976	1803	Kanigen	59 s pp	3-37, 44-60
31 Jan 1978	1841	glass	60 s pp	8-39, 44-64
7 Nov 1979	2053	glass	3 s Al	8-100[b]
16 Nov 1979	1703	Kanigen	3 s Al	3-100[b]
13 Feb 1981	1916	glass	45 s pp	8-39, 44-64

a. pp is nominally 1 micron of polypropylene (C_3H_6) coated with 1500 Å of Al plus a 1500 Å Al prefilter. Al is 1500 Å of aluminum without a prefilter.

b. The sensitivity of the photographic emulsion at the long wavelength cut-off is unknown and may well limit the bandpass to shorter wavelengths.

REFERENCES

Allen, C.W.: 1963. Astrophysical Quantities, Athlone Press, London, 179.

Bohlin, J.D.: 1977 in J.B. Zirker, (ed.) Coronal Holes and High Speed Wind Streams, Colorado Associated University Press, Boulder, 27.

Davis, J.M., Golub, L., and Krieger, A.S.: 1977, Astrophys. J. 214, L141.

Giacconi, R., Reidy, W.P., Vaiana, G.S., Van Speybroeck, L.P., and Zehnpfennig, T.F.: 1969, Space Sci. Rev. 9, 3.

Glackin, D.L., Linsky, J.L., Mango, S.A., and Bohlin, J.D.: 1978, Astrophys J. 222, 707.

Goldberg, L.: 1939, Astrophys. J. 89, 673.

Harvey, J., Krieger, A.S., Timothy, A.F., and Vaiana, G.S.: 1974, Osserv. Mem. Oss. Arcetri 104, 50.

Harvey, J.W., and Sheeley, N.R., Jr.: 1977, Solar Phys. 54, 343.

Harvey, J.W., and Sheeley, N.R., Jr.: 1979, Space Sci. Rev. 23, 139.

Huber, M.C.E. et al.: 1974, Astrophys. J. 194, L115.

Levine, R.H.: 1982, Solar Phys. 79, 203.

Levine, R.H., Altschuler, M.D., Harvey, J.W., and Jackson, B.V.: 1977, Astrophys. J. 215, 636.

Mango, S.A., Bohlin, J.D., Glackin, D.L., and Linsky, J.L.: 1978, Astrophys. J. 220, 683.

Maxson, C.W., and Vaiana, G.S.: 1977, Astrophys. J. 215, 919.

McIntosh, P.S., Krieger, A.S., Nolte, J.T., and Vaiana, G.: 1976, Solar Phys. 49, 57.

Milkey, R.W.: 1975, Astrophys. J. 199, L131.

Milkey, R.W., Heasley, J.N., and Beebe, H.A.: 1973, Astrophys. J. 186, 1043.

Nolte, J.T., Davis, J.M., Gerassimenko, M., Lazarus, A., and Sullivan, J.D.: 1977, Geophys. Res. Lttrs. 4, 291.

Nolte, J.T., Krieger, A.S., Timothy, A.F., Vaiana, G.S., and Zombeck, M.V.: 1976, Solar Phys. 46, 291.

Sheeley, N.R., Jr., and Harvey, J.W.: 1981, Solar Phys. 70, 237.

Shine, R., Gerola, H., and Linsky, J.L.: 1975, Astrophys. J. 202, L101.

Vaiana, G.S., Reidy, W.P., Zehnpfennig, T., Van Speybroeck, L., and Giacconi, R.: 1968, Science 161, 564.

Vaiana, G.S., Van Speybroeck, L., Zombeck, M.V., Krieger, A.S., Silk, J.K., and Timothy, A.: 1977, Space Sci. Instrumentation 3, 19.

Zirin, H.: 1975, Astrophys. J. 199, L63.

Zirker, J.B. (ed.): 1977, Coronal Holes and High Speed Wind Streams, Colorado Associated University Press, Boulder.

FIGURE CAPTIONS

Figure 1. Top: The comparison of the aligned X-ray and 10830 Å images and coronal hole boundaries for 27 June 1974. The 10830 Å boundaries are shown in the middle panel by heavy lines, the X-ray boundaries by light lines. Hatched areas indicate uncertain X-ray holes. The north and south poles are indicated by the vertical marks on the limbs of the middle panel.

Bottom: The same for 13 February 1981. The heavy dotted lines are uncertain boundaries of 10830 Å holes. The 10830 Å boundaries are projected on the X-ray image.

Figure 2. Top: The X-ray image and comparison of X-ray and 10830 Å coronal hole boundaries for 31 January 1978. The 10830 Å boundaries are projected back in time from the 1729 UT image of 2 February 1978 using the Newton-Nunn differential rotation rate. The 10830 Å hole boundaries are projected on the X-ray image.

Bottom: The same for 7 November 1979. The 10830 Å hole boundaries have been projected forward from the 1825 UT image of 5 November 1979 and backward from the 1732 UT image of 9 November 1979 using the Newton-Nunn rotation rate. Both sets of boundaries are shown.

Figure 3. The same as Figure 1 for 16 September 1976 (top) and 16 November 1979 (bottom). The 16 November 1979 image is a composite of two images at the times shown.

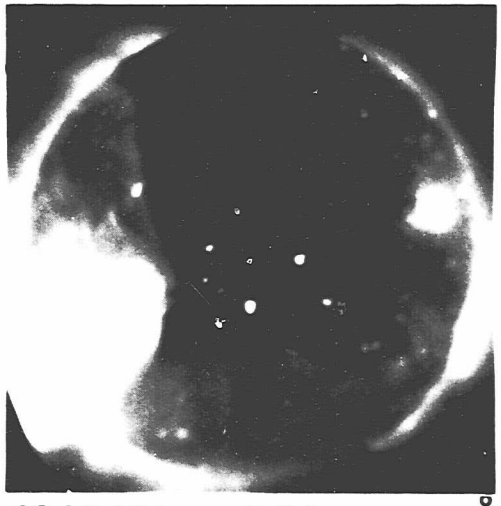

1948 UT 8-39, 44-64 Å

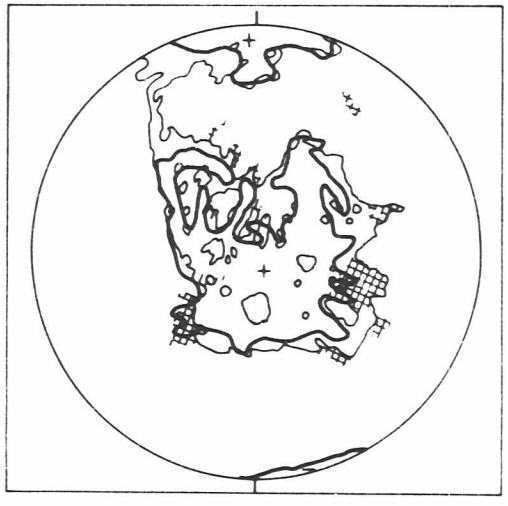

27 JUNE 1974

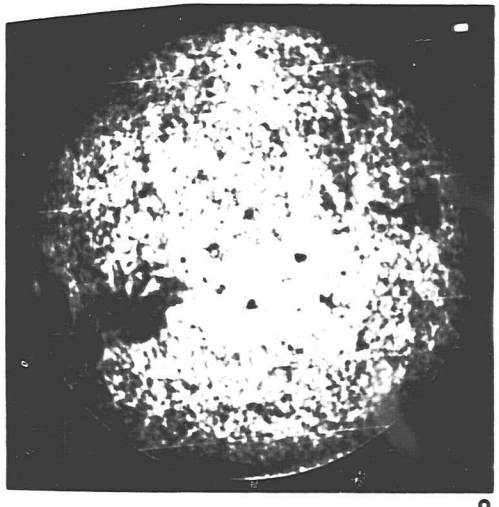

1637 UT 10830 Å

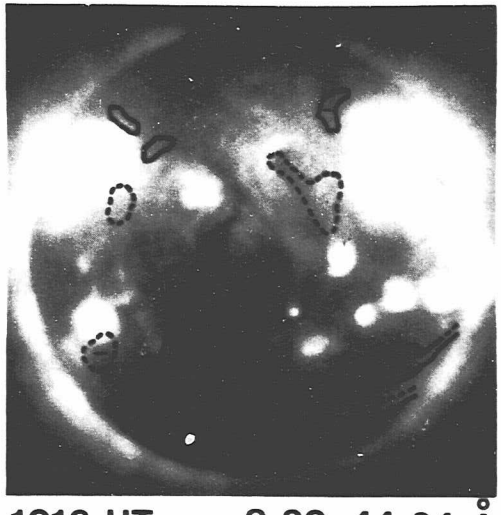

1916 UT 8-39, 44-64 Å

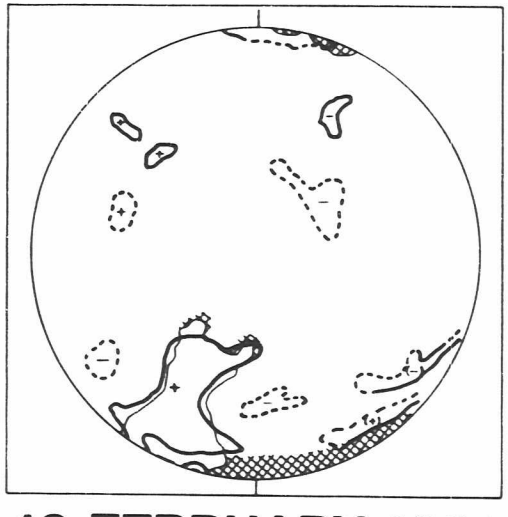

13 FEBRUARY 1981

1618 UT 10830 Å

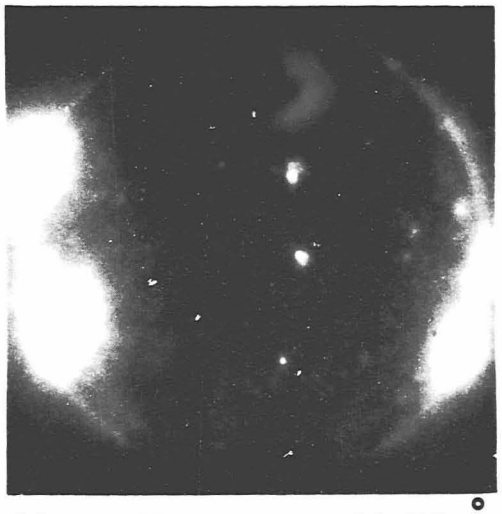

1803 UT 3-37, 44-60 Å

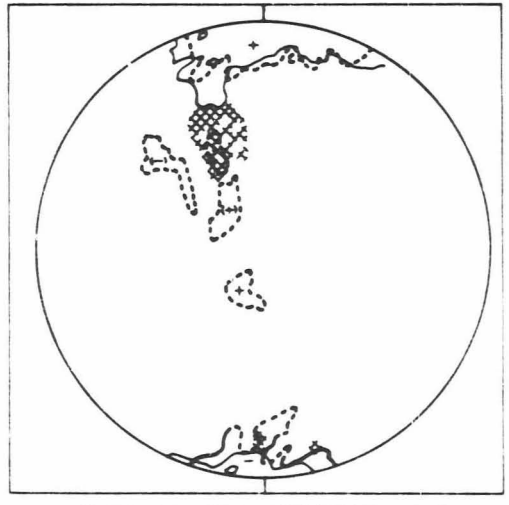

16 SEPTEMBER 1976

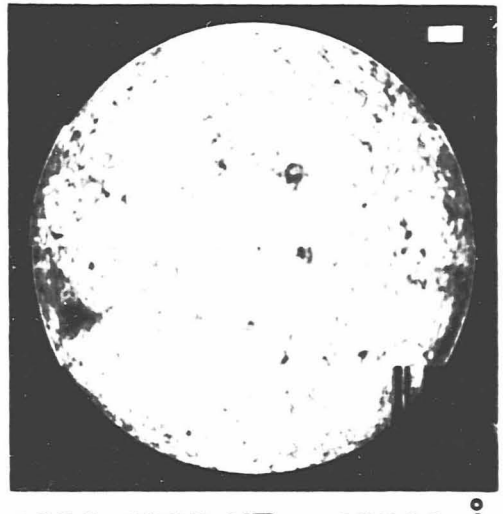

1630, 1822 UT 10830 Å

1703 UT 20-100 Å

16 NOVEMBER 1979

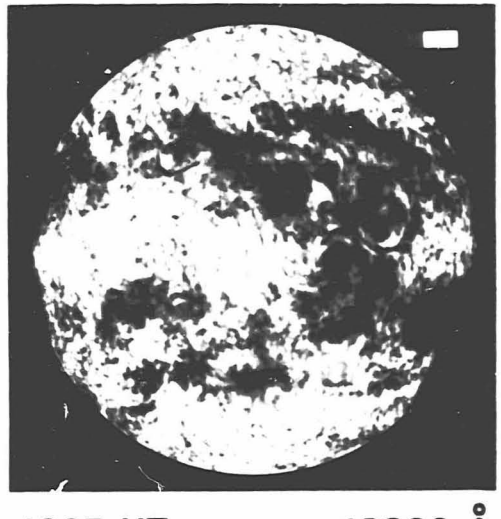

1627 UT 10830 Å

4.3 The Reappearance of Polar Coronal Holes and the Evolution of the Solar Magnetic Field

D.F. Webb and J.M. Davis

American Science and Engineering, Inc.
Cambridge, MA

and

P.S. McIntosh

Space Environment Lab/NOAA
Boulder, Colorado

ASE-4793

THE REAPPEARANCE OF POLAR CORONAL HOLES AND THE EVOLUTION OF THE SOLAR MAGNETIC FIELD

by D.F. Webb and J.M. Davis

American Science and Engineering, Inc.
Cambridge, MA 02139

and

P.S. McIntosh
Space Environment Lab, National Oceanic
and Atmospheric Administration
Boulder, CO 80303

To be Submitted to Solar Physics

March 1983

ABSTRACT

We examine observations relating to the polar evolution of the solar magnetic field around sunspot maximum, when the net polar flux reverses polarity and coronal holes redevelop around the poles. Coronal hole observations during the last two solar maxima are emphasized since sufficient synoptic, high-spatial resolution coronal emission data have been available only since the mid-sixties. Long-term averages of the latitudinal dependence of the photospheric magnetic field and the evolutionary pattern of the polar crown of Hα filaments are used as tracers of the poleward evolution of the reversal of the large-scale field, and are compared to the redevelopment of the polar holes. The polar holes reappear following the appearance of small, mid-latitude holes of new-cycle polarity which expand in longitude and poleward until they join and encircle the pole. We find that the appearance of these mid-latitude holes, the peak of flux emergence at low latitudes, and the polar polarity reversal all occur within a few solar rotations. Lagging 6 mo to 1 $^1/_2$ yr. after this time, the polar crown disappears and the polar holes redevelop.

We compare our results with Babcock-type models of the solar cycle, and emphasize the following complications to such simple scenarios. 1) The process of polarity reversal and redevelopment of the polar holes is discontinuous, occurring in 2 or 3 longitude bands, with surges of flux of old-cycle polarity interrupting the poleward migration of new-cycle flux. 2) Contrary to the Babcock hypothesis, the polar crown disappears months after the magnetic polar reversal. We suggest that there must be sufficient new-cycle flux poleward of the polar crown to cause an early reversal of the net flux. 3) The polar evolution at maximum was similar for the last two cycles, despite a significant diference in the rate and amount of flux emergence.

1.0 INTRODUCTION

Solar dynamo theories predict that the sun has a deep-seated dipole field oriented along the rotation axis with strong, unipolar fields at the poles. Babcock's model (1961) for the evolution of the solar magnetic field specifies that the polar fields will be strongest at solar minimum. Because coronal holes form in regions where the large-scale field is unipolar and the coronal density is low, we expect the poles to be covered by holes at solar minimum and this has been consistently observed (Waldmeier, 1981; Sheeley, 1980; Nolte et al, 1977). The persistence and large area of these polar holes indicate that most of the polar field has an open geometry. Recent phenomenological models of the formation and development of coronal holes (e.g., Bohlin and Sheeley, 1978; Hundhausen, 1977) have supported Babcock's ideas.

In essence these models imply the following scenario for the evolution of magnetic flux at the poles. First, BMRs (bipolar magnetic regions) of the new cycle erupt at low to medium latitudes. The trailing part of this new flux gradually moves toward the poles, canceling the unipolar field and reducing the open field area. The polar holes shrink in area until around the time of sunspot maximum the net polar flux is nearly zero and polar holes are small or nonexistent. Eventually sufficient flux of the trailing polarity of the BMRs accumulated at the poles to switch the net polarity, the polar field strengthens again, and the polar holes reform and grow.

This period of polarity reversal leading to the rebirth and development of the polar holes is clearly fundamental to our understanding of the evolution of the large-scale solar magnetic field. Observations bearing on the evolutionary sequence of the rebirth of the polar holes using various tracers of the magnetic field can provide such insight. However, since this period is short-lived, 1 - 2 yrs., relative to the entire cycle (Waldmeier, 1981) and since synoptic coronal observations have not been available until recently, observations of this important phase of the solar cycle have been minimal.

Since the mid-sixties, high spatial resolution coronal emission data as well as other forms of data have been available to study the solar cycle. Sufficient time has now elapsed to permit us to study for the first time two consecutive cycles of polar hole development around solar maximum.

The purpose of this study is to describe the evolution of the high latitude and polar magnetic field around solar cycle maximum and to relate these observations to models of the solar cycle, particularly dynamo models. A primary tool for this purpose will be the derivation of the relative timing near the maximum of the cycles 20 and 21 of five specific events; i.e., the peak of the sunspot number, the magnetic polarity reversal above 70° latitude, the disappearance of the polar crown of filaments, the first appearance of a small, mid-latitude coronal hole(s) of new-cycle polarity, and the encirclement of the pole by a hole. It will be shown that each of these events can be determined within a few solar rotations with our data set.

Hundhausen et al., 1981 (hereafter HHH) and Broussard et al., 1978 have shown that "mid-latitude" holes (those centered at latitudes roughly between 20 and 60°) were a feature of the corona during the maximum of cycle 20. In Section 2 we show that one of the characteristics of the post-maximum coronal evolution of the last 2 cycles was the areal increase and poleward growth of particular mid-latitude holes of new-cycle polarity to become large "high-latitude" holes (centered at latitudes $\gtrsim$ 50-60°), which eventually encircled the poles. For cycle 20 this process in the southern hemisphere is described in detail as an example of our technique. In Section 3 we describe the evolution of the high latitude magnetic field using measurements of the migration of the polarity reversal of the photospheric field and of the migration and dissolution of the polar crown. In Section 4 we summarize our results and discuss their implications for models of the solar cycle.

2.0 HIGH LATITUDE CORONAL HOLE EVOLUTION AROUND MAXIMUM

Figure 1 is a superposition of the rise, maximum and early decline phases of cycles 20 and 21 using smoothed values of R_Z, the Zurich sunspot number, normalized to their starting minima in October 1964 and June 1976.

The maximum of cycle 20 was broad, with shape and peak similar to the average profile of the previous 12 cycles. In contrast, cycle 21 was one of the most active, in terms of sunspot number, in recent times. Compared to cycle 20 it had a steeper rise and an earlier and narrower peak. If Babcock-type models of the solar cycle are valid, we might expect to observe distinctly different patterns of evolution in the polar regions for two cycles with such different levels and distributions of magnetic activity. In the next two sections we will attempt to study the process of emerging and evolving solar magnetic fields by describing the evolution of high-latitude coronal holes leading to the reformation of the polar holes.

The data used in this study consisted of the following. Coronal data included AS&E X-ray rocket images (the times are indicated by the vertical lines on Figure 1), Harvard OSO-6 Mg X maps in cycle 20, and HAO white light eclipse image on 7 March 1970, synoptic HAO white light K-coronameter charts for cycle 20 and synoptic He I-10830Å coronal hole boundaries for cycle 21. Various formats of NOAA/SEL Hα synoptic charts were used to trace the poleward migration of filaments and of the large-scale field. Graphs of the latitudinally averaged photospheric field from Mt. Wilson were used to trace the poleward migration of the polarity reversals at the times of maxima.

2.1 The Redevelopment of the Polar Holes in Cycle 20

During cycle 20 the sunspot number was highest from 1968 to mid-1970, after which it declined rather rapidly (Figure 1). The difference in the solar corona, especially coronal holes, before and after mid-1970

was dramatic. The structure of the solar crown during the maximum of cycle 20 was observed in 1969 with the use of K-coronal observations (HHH) and EUV and soft X-ray images obtained by rocket flights (Krieger et al., 1971 - Figure 6 and Broussard et al., 1978). The rocket images corroborate the description given by HHH: the corona was characterized by (1) the absence of polar holes, (2) the presence of elongated mid-latitude holes, and (3) a fairly random mixture of dominant magnetic polarities in the northern and southern hemisphere. In particular, the AS&E X-ray image on 4 November 1969 (Carrington Rotation 1554) showed that there was no pole-encircling coronal hole in the south in 1969 until after November.

Then when did the polar holes reappear in cycle 20? We will emphasize observations of the south polar hole, both because it reappeared first and was preceded by more systematic coronal hole development than in the north. Although HHH claim that "true" polar holes were still absent from their synoptic charts through 1970, they noted that by mid-1970 (CR 1561-63) magnetic dominance by a single polarity in each hemisphere had begun to appear. The polarities (positive in the north, negative in the south) were as expected for the new cycle following maximum.

A large, high-latitude hole covering the south pole over half a solar rotation is evident on the K-coronameter maps at least as early as July 1970 (CR 1563). By October 1970 (CR 1567) the south pole was completely encircled by a hole.* This encirclement is supported by the observation of an unambiguous polar hole and extension to the equator at about L = 270° on the AS&E X-ray image taken on 24 November 1970 on CR 1568 (Krieger et al., 1973). This asymmetric polar hole with its

---

* HHH claimed that this encirclement did not occur until early 1971 (CR 1572). After analysis of their published maps, we believe that the encirclement actually occurred much earlier.

equatorward extension was a continuous feature of the corona back to July 1970.**

What can we say about the critical period of late 1969 to mid-1970 when relatively rapid changes were apparently occurring in the sun's global magnetic field? We have been able to establish the general evolution of coronal holes and the global field during this period by the use of a cine presentation of the corona obtained with the Harvard spectroheliograph on the OSO-6 satellite (Withbroe, 1981), Hα synoptic charts (McIntosh, 1979), and coronal data obtained on 7 March 1970, the day of a total solar eclipse at the earth.

On the OSO-6 movie we observed the gradual development of three coronal holes which we believe were the early coronal signature of the new-cycle polarity reversal in the southern hemisphere. These holes appeared at mid-latitude and expanded in longitude and toward the south until they reached the pole. All three holes were of negative polarity, the same polarity as the new-cycle flux in the south. The centroids of the holes were relatively stationary in longitudes, with average Carrington longitudes of 20, 110, and 220° (see Appendix). The hole at L ≈ 110° is of particular interest because it stretched across the central meridian on the day of the 7 March 1970 eclipse and hence was well observed. It was bounded in the south by the polar crown until March 1970 (CR 1558) when the polar crown began to break up. An Hα image on 7 March 1970 and the synoptic chart for CR 1558 show a gap near the pole between filaments from L85° and L145° (Figure 3). It is possible that the L = 110° hole connected to the pole on CR 1558 and in fact may have been joined to the L ≈ 220° hole observed at the west limb on 7 March 1970.

**It was identified with the first long-lived, recurrent high speed wind stream following solar maximum (Krieger et al., 1973; Sheeley et al., 1977). The stream first appeared on August 1970 (CR 1564), in agreement in time, polarity and longitude with the southern coronal hole.

The eclipse data help to clarify these connections. Figure 2 is a superposition of the 7 March AS&E X-ray image of the inner corona and the HAO ground-based white light image of the outer corona. Let us focus on the SW quadrant of this figure. The X-ray image revealed large areas of low emission, similar in appearance to coronal holes, surrounding both poles. In March the solar B_0 angle had its maximum negative value, so that the south pole was visible to us. Gaps in the X-ray limb emission occurred at position angles of 180° and 215-240° (measured CCW from north). They corresponded to gaps in the white light emission (Van Speybroeck et al., 1970; HHH), the former to a small hole near the south pole and the latter to the large hole at L ≈ 220° (Appendix). In X-rays the region between these two "accepted" holes contained a band of similar low emission, giving the appearance of a continuous high-latitude hole with a connection to the pole. There is no evidence that the helmet streamer lying at 180-215° had its base on the front side of the disk as suggested by HHH. We believe this feature likely overlaid a filament channel on the hidden hemisphere.

Figure 3 shows the Hα synoptic map for CR 1558. The top map has superimposed on it the boundaries of the coronal holes drawn from the 7 March 1970 X-ray image (Figure 2) using a Stonyhurst disk as an intermediary. In the coronal images projection effects can obscure the hole boundaries, especially at the poles during solar maximum. The double dashed lines mark regions where filament arcades caused such obscuration. The bottom map shows the 2 and 3 x 10^{-8} pB K-coronameter contours from the west limb data of HHH. Comparison of these maps reveals that 1) in the southern hemisphere the 3 x 10^{-8} pB contour lies within the negative polarity cell, 2) that part of the southern coronal hole visible on the X-ray image is of uniform darkness and its boundary generally follows that of the 3 x 10^{-8} contour, 3) the small positive polarity hole near the center of the X-ray disk (S25, 135°L) is not visible in the white light data, and 4) although the north polar region was poorly observed at this time, the X-ray image revealed low emission over the pole that could have been a coronal hole. It is likely that the area between L = 60 and L = 190° in the K-coronameter data was

obscured by high, bright arcades overlying the neutral line at N50-60°. These observations suggest that the south pole at this time was encircled by a large, asymmetric hole of negative (new-cycle) polarity. We suggest that by March 1970 the large-scale polar field was already dominated by the polarity of the new cycle, but contained an admixture of opposite field producing some faint emission from closed structures.

The above comparison shows that at this time of the cycle the 3×10^{-8} pB contour of the K-coronameter data more closely represents the location of the polar hole. Because HHH used the 2×10^{-8} contour to define coronal holes, they concluded that there were no polar holes on 7 March. In addition, we believe that HHH's interpretation of the timing of the reappearance of the polar holes was overconservative. Their use of a single, average contour to define hole boundaries over the entire cycle and to define polar encirclement only when the pole appeared to be surrounded by a fairly wide, uniform band of low emission yields estimates of polar hole rebirths which are consistently many rotations later than our deductions of the earliest encirclement. HHH's conservative approach is understandable given the limitations of the K-coronameter data, which they discuss in detail. We note that these data are particularly insensitive to the detection of small coronal holes and of the accurate boundaries of large holes, especially those obscured by brighter structures in the line of sight. These problems are more severe at solar maximum near the poles where the pB signal contains a large contribution due to numerous bright structures in the mid-latitudes.

We will briefly summarize the evolution of high-latitude holes in the northern hemisphere, where this process was more complicated than in the south. HHH noted that redevelopment of the north polar hole occurred in a manner similar to that in the south during cycle 20. Namely, a small positive polarity (new-cycle) hole developed at mid-latitudes and expanded towards the pole to eventually encircle it. However, the process lagged that of the south and took longer. The

evolutionary patterns in the north were not as straightforward as in the south, apparently having been complicated by a "wave" of late-emergent flux (e.g., Waldmeier, 1973).

We interpret the K-coronameter maps as indicating that the northern pole was encircled by a hole by CR 1572-73 rather than by CR 1574 as suggested by HHH, and that this event was preceded by the growth of a high-latitude hole which developed on or before CR 1561 (May 1970). HHH thought this hole disappeared then reappeared between CR 1567 and 1570. But we feel the positive polarity hole only temporarily fluctuated in area, possibly because of a surge of negative flux which swept through the northern mid-latitudes in 1970 (Howard and LaBonte, 1981).

In summarizing the developments in cycle 20, we conclude that the south polar hole redeveloped first, starting with the birth of mid-latitude holes in late 1969. These evolved into three holes dominating most of the region south of latitude S40-50°, each with connections to the pole by March-April 1970. At this same time the south polar crown began to break up (Section 3) and by CR 1561 it was gone, implying the pervasiveness of new-cycle flux at that time. This process took longer in the north, lagged that of the south and was more complicated. A persistent, positive polarity mid-latitude hole did not appear in the north until mid-1970, following by half a year the development of such a hole in the south. The polar hole redeveloped in the spring of 1971, nearly one year later, whereas this process took only 5-6 months in the south.

2.2 The Redevelopment of the Polar Holes in Cycle 21

We now extend our discussion to the rebirth of the polar holes following the sunspot maximum of the present cycle, cycle 21. Referring again to Figure 1 we see that the sunspot number peaked in December 1979, and that the peak was sharper and higher than in cycle 20. AS&E X-ray rocket images of the sun were obtained at the maximum, and early into the declining phase of the cycle, as denoted by the vertical lines on the Figure. In addition, Hα , magnetogram and He I - 10830 Å data were

available for each flight, and synoptic charts of these data (Solar-Geophysical Data) were used in our analysis.

Figure 4 presents the AS&E X-ray images obtained on 7 November 1979 (a), near solar maximum, and on 13 February 1981 (c), 14 months after maximum. These images had similar sensitivities at the film plane and covered similar solar longitudes (CMP ≈ 300°L for both images). At the bottom of the figure are tracings of the boundaries of the darkest areas on the X-ray images, and tracings from Hα synoptic charts for CR 1688 and 1705 of the definite (solid) neutral lines and filaments which were located near the dark X-ray features. Since neutral lines tend to border coronal holes and lie within coronal cavities (e.g., McIntosh et al., 1976), they help us to separate these two types of dark X-ray features.

No polar holes are evident on the 7 November 1979 image, nor on another X-ray rocket image obtained on 16 November 1979. Together these images provided coverage of approximately 2/3 of the solar disk near solar maximum. The dark lanes near the poles corresponded to polar crown or high-latitude filament channels. A small hole may have appeared near the south pole on 16 November, but it was probably of negative polarity, i.e., indicative of old-cycle flux. Small mid- and high-latitude coronal holes appeared on both images.* We conclude that the overall appearance of the low corona at the maximum of cycle 21 was similar to that of cycle 20. Namely, there were small mid-latitude holes but no conspicuous polar holes, and no large-scale organization of magnetic polarities in the north and south.

---

*In a recent comparison of these and earlier AS&E rocket X-ray images with KPNO 10830 Å images, Kahler et al. (1983) found that the brightness contrast between large-scale coronal structure and holes decreased toward solar maximum. Also, from 1976 to 1981 mid- and low-latitude holes were generally small and of low contrast, and there was poor agreement between X-rays and 10830 Å in the location and boundaries of these holes.

However, by the time of the February 1981 image a large, asymmetric coronal hole extended to near the south pole. Note that, as in March 1970, the solar south pole was visible on the disk. A possible coronal hole was associated with the north pole, but this is uncertain because that pole was tilted away from the earth.

Figure 5 combines coronal hole boundaries from daily KPNO He I-10830 Å images with the patterns of magnetic polarity from Hα synoptic charts of the southern high latitude zone S30-70° for CR 1682 - 1725. This period begins just before sunspot maximum and extends well into the declining phase. Several important evolutionary patterns are evident in this figure. During the period shown in Figure 5a, a high latitude negative-polarity hole disappeared about the time of sunspot maximum. The south polar region gradually became dominated by positive, new-cycle polarity. The coronal hole visible on the February 1981 X-ray image was of new-cycle polarity and experienced a steady growth in longitude and poleward from the time of its birth as a mid-latitude hole on CR 1695, only 6 months after maximum. The poleward boundary, typically marked by the polar crown, between the old and new-cycle flux shrank poleward until it disappeared above S70° on CR 1701 and disappeared as a conspicuous encircling crown on CR 1707 (see Section 3.2). By about January 1981 the sun had become encircled by positive polarity at high southern latitudes, which were dominated by the coronal hole between S50 and 70°. This hole was largest on CR 1707-1708, possibly with connections to the pole.

This episode was followed by a poleward surge of negative polarity flux from CR 1709 to 1722 which coincided with a large reduction in the high latitude hole area. The surge is seen as increased black polarity at high latitudes in Figure 5 and as a prolonged negative downturn in the magnetic field averages at mid- to high-latitudes (Figure 6; Section 3.1). It is evident from Figure 6 that, like the earlier polarity reversal, this negative surge began at lower latitudes and progressed steadily poleward. It was contemporary with the development of a second mid-latitude hole on about CR 1714 at L ≈ 260°. Like the first such hole, this hole grew in size and expanded poleward until it connected to a polar

segment on CR 1723. Because the reduction of the high latitude hole area occurred during a period when the north pole was tilted away, we cannot be sure when the pole became encircled by a hole. By CR 1717, when the B_o angle was again favorable, the pole was definitely encircled.

The evolutionary process in the north was as complex as that in the south. However, with the possible exception of the development of the polar hole, the reversal process began first in the north in contrast to the situation in cycle 20. A north polar diagram for the latitude zone N30-70°, similar to Figure 5 and covering the same period, was prepared but is not shown here. The diagram reveals that the northern hemisphere was encircled by negative, new-cycle polarity flux at high latitudes by CR 1690, about the time of the sunspot maximum in December 1979. On this same rotation a small hole appeared stretching from about N35 to 55°, and on subsequent rotations it expanded in longitude, then shrank and disappeared on CR 1698, last being visible at about 270°L. On CR 1695 another small hole appeared at 130°L and expanded rapidly to encircle about half the sun, probably approaching very near to the pole on CR 1699. By CR 1712 the pole was completely encircled by a hole. In the interval CR 1700-1712 the situation was confused, probably because of another poleward surge of flux. This surge occurred from about CR 1708 to 1714 and is seen as increased white (positive) polarity at high latitudes in the zonal plots and as a positive poleward moving peak in the magnetic field averages (Figure 6). During this period the north pole might have been encircled by a hole; the daily 10830 Å images showed evidence for a small hole near the pole of small size and longitudinal extent.

Summarizing cycle 21 we find that both polar holes redeveloped at about the same time, in mid to late 1981, following by 1- $1\frac{1}{2}$ yr. the appearance of persistent mid-latitude holes of new-cycle polarity. The magnetic reversal process in the north preceeded that is the south by about 6 mo., as did the polar crown disappearance. In each hemisphere the complete encirclement of the pole was delayed by surges of late-emergent flux.

3.0 THE POLAR MAGNETIC FIELD EVOLUTION AROUND MAXIMUM

So far we have discussed the period of reversal of the sun's poloidal field mainly in terms of the redevelopment of the polar holes. However, there are specific tracers of the evolutionary pattern of the magnetic flux that can be related to the polar evolution of maximum. These data include plots of the time of reversal of the long-term average field strength as a function of latitude, and the evolution of the polar crown of filaments. Below we discuss each of these tracers for the last two cycles and relate them to the rebirth of the polar holes.

3.1 The Magnetic Polarity Reversal

Probably the most detailed discussion of the polar polarity reversal during cycle 20 was given by Howard (1972; 1974). Using Mt. Wilson magnetograph data, he produced plots vs. time of the average field in discrete latitude intervals. With these data he observed successive reversals of the sign of the field to the new-cycle polarity starting at 40-50° latitude and proceeding to the pole. The time for this "migration" was 1 to 1 1/2 yr. and the pattern was observed at both poles, although not at the same time. The reversal occurred at least 11 rotations earlier in the south than in the north, in agreement with the pattern of the development of the high-latitude and polar coronal holes.

R. Howard has kindly provided Figure 6, which is a plot of the north and south field averaged over six latitude intervals from 1978 to 1982. The plot is similar to those in his 1974 paper. Although the data contain significant fluctuations and the zero level is uncertain, we can see that a long-term reversal to new-cycle polarity (negative in the north, positive in the south) occurred above latitudes 70° around March 1980 in the north and about 6 months later in the south. Because the polemost latitude band that the magnetograph samples is so large, these measurements underestimate the time of reversal at the pole. However, the poleward reversal "wave" moves so rapidly in each hemisphere that the actual polar reversal is probably underestimated by only 1-2 rotations. A tendency for earlier reversal at successively lower latitudes is also apparent.

As we mentioned earlier the timing of the reversals in cycle 21 was complicated by apparent poleward surges of old-cycle polarity flux in both hemispheres. This occurred earlier and was more clearly delineated in the north. The northern surge also produced a clear but temporary positive shift in the long-term increasingly negative polar field. However, the effect of this shift in the polar field was very weak and the second "reversal" was out of phase with the timing of the other tracers. Therefore, although in Table I we have listed two times when the field >70° reversed polarity from positive to negative, we conclude that the earliest reversal was the "true" one. The southern surge did not appear to be strong enough to reestablish negative flux above 70°S, so we list only one reversal time for the southern hemisphere.

Table I lists the times of polarity reversals above latitudes 70° for cycles 20 and 21. We see that in cycle 20 the south pole reversed at least 3/4 yr. before the north, and in cycle 21 the north pole reversed first about 1/2 yr. before the south. For both cycles the general pattern of development of new-cycle polarity coronal holes followed these reversals in this same sequence. These observations are therefore consistent with our expectation for the general evolution of the polar field following maximum set forth in the Introduction. For completeness we have included in Table I Babcock's (1959) estimate of the time of reversal during cycle 19 when the south reversed about 1 1/2 yr. before the north.

3.2 The Disappearance of the Polar Crown

The poleward migration of the polar crown of filaments is one of the key observational parameters that must be accounted for in models of the solar cycle (e.g., Leighton, 1964). After sunspot minimum filaments in the mid-latitudes begin to move toward their respective poles. The locus of filaments maintains a nearly constant distance of 20° from the boundary of the shrinking polar hole (Waldmeier, 1981); in fact the coronal arcades overlying the filaments form the physical boundary of the polar hole (McIntosh et al., 1976). For the past several cycles the reappearance of the polar holes has occurred close to the time of arrival near the pole and disappearance of the polar crown (Waldmeier, 1981).

We have determined the time of disappearance of the polar crowns for cycles 20 and 21 through the use of Hα synoptic charts (McIntosh, 1979; Solar Geophysical Data) and high-latitude zonal diagrams, like Figure 5, which are derived from the Hα charts. The method of producing these charts is discussed by McIntosh (1972a; 1972b). McIntosh (1980) describes the method of producing the zonal diagrams and gives an example of the south high-latitude zone for the years 1967-69. The zonal diagrams are produced by shading opposite polarity regions in narrow bands of latitude, then assembling them in time series. Although the locations of filaments and neutral lines at latitudes higher than about 60° is uncertain, daily mapping tends to minimize such errors. This method permits us to observe the systematic progression of features on the maps. For instance, on Figure 5 we can determine when the polar crown moved to latitudes higher than 70° by observing that the last vestige of black polarity disappeared from the bottom of the zone on CR 1701.

Using mean values of the latitude distribution of prominence areas, Waldmeier (1973) was able to determine the poleward migration rate and time of arrival at the pole of the polar crown for cycle 20. Using the Hα synoptic charts, we have developed similar curves for cycles 20 and 21 which show the maximum latitude reached per rotation of the polar crown. The times of polar crown disappearance listed in Table I were determined to be the rotation on which the last conspicuous polar crown filament was observed.* The disappearance times for cycle 19 were estimated from Waldmeier's (1981) Figure 5. For cycle 21 complete sets of limb promi-

---

* From Waldmeier's (1973) data on the evolution of the northern polar crown in cycle 20 one would infer an earlier disappearance time than ours. This is because his "anamalous" polar crown (also referred to by Howard, 1974) was not the final one. Following the passage of the "anomalous" front the polar field was negative-polarity which then switched to the new-cycle (positive) polarity after the passage of the final polar crown.

nence photographs were available. Observations of the dissolution of polar prominences can be a more sensitive way of inferring the polarity reversal. In cycle 21 the last conspicuous prominence at each pole was observed 1 1/2 - 3 mo. after the times in Table I. However, we believe the times in Table I better represent the average time for the inferred reversal.

4.0 SUMMARY AND DISCUSSION

4.1 Summary of Results

We will now attempt to synthesize these observations in order to learn more about the polar evolution of the solar magnetic field. Several caveats are required for the interpretation of these data: 1) Like other solar synoptic observations, the data are noisy and only longer term trends can be discerned. This is especially true of the polar observations which are effected by foreshortening and the tilt of the solar axis with regard to the ecliptic; 2) As noted by Howard (1974) the timing of the magnetic polarity reversal is uncertain, requiring several years of data around solar maximum to asertain when it actually occurred; 3) Coronal hole boundaries were determined from different sets of data in cycles 20 and 21. In cycle 20 we used higher altitude K-coronameter, X-ray and EUV data and in cycle 21 we used primarily lower altitude He I-10830 Å data. The detailed intercomparison of hole boundaries determined at these different wavelengths is not well understood, but the general location and evolution of the larger holes should be sufficiently accurate for our purposes; 4) Because of these limitations we estimate that the uncertainties in the timings of Tables I and II are of the order $\pm$ 2 rotations.

We will synthesize these observations by relating the timing of the key high latitude events to the polarity reversals. Table II is adapted from Table I. It shows the lag times in Carrington rotations from the time of the earliest indication of the polarity reversal above 70° in each hemisphere to the time of the following events: the development of

the mid-latitude hole of new-cycle polarity, the disappearance of the last conspicuous polar crown filament, and the polar encirclement by a hole. In overview we can summarize these results as follows. The peak of the flux emergence at low latitude (in terms of sunspot number), the appearance of the mid-latitude hole, and the polarity reversal at the pole all occurred within a few months of each other. This is particularly true if we compare the time of the earliest indication of the polar reversal and the earliest birth of a mid-latitude hole. The polar crown disappearance and the redevelopment of the polar hole occurred about 6 mo. to $1\frac{1}{2}$ yr. after the polar reversal. Polar hole encirclement occurred just before the time of polar crown disappearance in cycle 20, and after it in cycle 21, lagging by about one year in the north. For the last two cycles the relative timing of these events, with the possible exception of polar hole encirclement, appears to be consistent despite the obvious difference in the peak and shape of the sunspot numbers of the cycles.

4.2 Discussion

We have examined the observations relating to the evolution of the high-latitude solar magnetic field around sunspot maximum, when the net polar flux switches polarity and coronal holes redevelop around the poles. We will attempt to describe this process in the context of the phenomenological description discussed in the Introduction.

Before activity maximum new-cycle flux in the form of BMRs emerges at mid-latitudes. The trailing part of this flux, of opposite polarity to that of the old cycle at the poles, moves toward the poles, canceling the unipolar field there and reducing or eliminating the area of the pole occupied by a coronal hole. Near sunspot maximum a sufficient amount of trailing polarity flux has arrived at the poles to switch the net flux to new-cycle polarity, although enough mixed polarity remains to prevent the formation of holes. In the mid-latitudes at this same time the field has reversed and the new-cycle flux is sufficiently dominant for small holes to form. After maximum, as the amount of new

flux brought to the surface begins to decline and the BMRs continue to move equatorward, large unipolar areas of new-cycle polarity begin to dominate the mid- to high-latitude region. In two or three longitude zones the small holes begin to enlarge. Although they can spread very rapidly, for a period of time they are prevented from encircling the sun at high latitudes because of residual flux emergence and poleward flows or surges of old-cycle flux. The holes persist and grow larger and their coronal emission decreases until they join at high latitudes to completely encircle the pole. At about this time the polar crown, which is supposed to form the boundary between the old-cycle or mixed polarity of the pole and the new-cycle, high-latitude polarity, begins to break up and disappear as it nears the pole. Although the development time of the new-cycle, high-latitude holes for these two cycles varied from 6 mo. to 1 $^1/_2$ years, the appearance of the polar hole occurred within a few rotations of the disappearance of the polar crown in both cycles.

In general, our results support the Babcock-type schematic and phenomenological models of the solar cycle. However, we note the following results of our detailed observations which imply a more complicated scenario at solar maximum.

First, the process of polarity reversal leading to the redevelopment of the polar holes is not a smooth process that sweeps the trailing flux from the emerging flux belts to the polar. Instead it is discontinuous, occurring in longitude bands about 180° apart. These patterns are apparent in the zonal synoptic maps, such as Figure 5, as longitudinal "flow" patterns in the opposite polarity flux regions and the coronal holes, leading to a "barber pole" effect. However, these longitudinal "flows" are actually fairly stationary, having a constant rotation rate, about 29 days, which is faster than the Carrington rate.

This periodic distribution is reflected in latitude as well and in all of the magnetic tracers that we have examined; i.e., coronal holes, latitudinally averaged photospheric magnetic fields, and the polar crown. This process is perhaps best seen in the coronal hole evolu-

tion. Small mid-latitude holes form. Eventually one or more of them continues to grow in area and to move poleward until a segment reaches the pole. This latter process yields the large, asymmetric, high-latitude holes discussed earlier and typical of high-latitude holes soon after maximum. The ultimate development of a symmetrical polar hole does not occur until a second poleward thrust of new-cycle flux as evidenced by the growth of a second mid-latitude hole. This second hole develops at a longitude 180° from the first, and lags the first by 5-10 rotations. The observed poleward "surging" of the old-cycle flux (Figure 6) after the early polar reversal and mid-latitude hole appearance tends to disrupt the growth of new-cycle flux, to maintain the asymmetry of the high-latitude holes, and to diminish the hole area. If the surge reaches the polar zone, the polar crown will be reestablished in that longitude band. This yields the kind of "anomalous" polar crown first reported by Waldmeier (1973) in the north in cycle 20.

Our second result concerns the relationship between the polar field reversal and the polar crown disappearance. The polar crown is hypothesized to form the boundary between the poleward-receding old-cycle flux and the advancing new-cycle flux. If this idea were correct, then we could use the time of disappearance of the polar crown to infer the time of polarity reversal at the pole. We can predict that this inferred time should be approximately the same as that implied by magnetograph polarity measurements. If the strongest new-cycle field lay 15-20° equatorward of the polar filaments, we might expect the measured reversal to lag the inferred reversal by several rotations. Howard (1974) first noted that for cycle 20 this relationship was not as good as expected. We have discovered that, for the last two cycles, the opposite actually occurred; i.e., the polar crown consistently disappeared 6 months to 1 year after the magnetic polar reversal.

How can we explain this surprising result? We suggest two possibilities: 1) The wave of polarity reversal may slow as it nears the pole, despite an apparent observed tendency for acceleration up to 70° latitude. This retardation could be caused by compression of the

polar field lines and strengthening of the polar (old) field before sufficient reconnection can occur to neutralize the field. There is, however, no evidence that the polar crown slows near the pole (e.g., Waldmeier, 1973). 2) There may be a sufficient admixture of new-cycle flux poleward of the polar crown to cause a net polarity reversal at the pole before the polar crown dissipates. If so this net flux imbalance might enhance the process of the polar crown dissolution by various reconnection processes (e.g., Hansen and Hansen, 1977), causing filament ejections and the establishment of unipolar field at the pole. In support of this idea, we observe that after reaching latitudes of ≈80° the breakup and disappearance of the polar crown ring proceeds rapidly within a few rotations. We might also expect to observe an increased number of high-latitude coronal transients around this time of the solar cycle.

Finally, we find it rather remarkable that the evolution of the polar field near maximum was so consistent in terms of the timing of the magnetic tracers (with the possible exception of the redevelopment of the polar holes and the polar crown disappearance in cycle 19 - South.) Babcock (1963) predicted that a strong initial magnetic field (at solar minimum) would lead to an early and higher solar maximum. Although sunspot numbers imply that the start of cycle 21 had only slightly more flux than cycle 20, approximately 60% more magnetic flux was present at the maximum of cycle 21 than cycle 20 (Howard and LaBonte, 1981). At first glance we might then expect all polar events to proceed more rapidly for the more "active" cycle as they seem to at lower latitudes. This is not the case. Although the polar reversal occurred faster in cycle 21 in accordance with the flux emergence, the timing of the mid- to high-latitude new-cycle flux domination and the polar crown migration and disappearance were consistent during the last two cycles. Polar hole encirclement was retarded in cycle 21. We can interpret this as due to the increased amount of flux emerging at low latitudes at solar maximum, with subsequent poleward surging of old-cycle flux disrupting the development of the high-latitude unipolar fields.

polar field lines and strengthening of the polar (old) field before sufficient reconnection can occur to neutralize the field. There is, however, no evidence that the polar crown slows near the pole (e.g., Waldmeier, 1973). 2) There may be a sufficient admixture of new-cycle flux poleward of the polar crown to cause a net polarity reversal at the pole before the polar crown dissipates. If so this net flux imbalance might enhance the process of the polar crown dissolution by various reconnection processes (e.g., Hansen and Hansen, 1977), causing filament ejections and the establishment of unipolar field at the pole. In support of this idea, we observe that after reaching latitudes of ≈80° the breakup and disappearance of the polar crown ring proceeds rapidly within a few rotations. We might also expect to observe an increased number of high-latitude coronal transients around this time of the solar cycle.

Finally, we find it rather remarkable that the evolution of the polar field near maximum was so consistent in terms of the timing of the magnetic tracers (with the possible exception of the redevelopment of the polar holes and the polar crown disappearance in cycle 19 - South.) Babcock (1963) predicted that a strong initial magnetic field (at solar minimum) would lead to an early and higher solar maximum. Although sunspot numbers imply that the start of cycle 21 had only slightly more flux than cycle 20, approximately 60% more magnetic flux was present at the maximum of cycle 21 than cycle 20 (Howard and LaBonte, 1981). At first glance we might then expect all polar events to proceed more rapidly for the more "active" cycle as they seem to at lower latitudes. This is not the case. Although the polar reversal occurred faster in cycle 21 in accordance with the flux emergence, the timing of the mid- to high-latitude new-cycle flux domination and the polar crown migration and disappearance were consistent during the last two cycles. Polar hole encirclement was retarded in cycle 21. We can interpret this as due to the increased amount of flux emerging at low latitudes at solar maximum, with subsequent poleward surging of old-cycle flux disrupting the development of the high-latitude unipolar fields.

Our observations appear to support recent studies of the magnetic field (Howard and LaBonte, 1981) and polar filaments (Topka et al, 1982) which suggest that there is a poleward meridional flow averaging about 10 m s^{-1}. These authors have interpreted this flow as the result of a large-scale poleward circulation that cannot be accounted for by Leighton (1964) - type diffusion. In the Mt. Wilson data the strongest flows originated in the sunspot belts near solar maximum and moved to the poles in 2-3 years. We see apparent poleward flows of this magnitude in our data at high latitudes near maximum. For instance, in the south in cycle 21 the polarity reversal wave and the subsequent surge of old-cycle flux moved poleward below 70° at about 13 m s^{-1}. And, although the coronal hole boundaries at high latitudes are difficult to measure, we estimate that the poleward movement of the high-latitude coronal holes was about 10-15 m s^{-1}.

We can ask what our data can tell us about solar cycle models. Unfortunately, such models generally are not sufficiently developed to predict activity on the time scales dicussed here. Our observations do show evidence of poleward meridional flows, which argue against Babcock-Leighton diffusion, a requirement of their dynamo model. Further, Howard and LaBonte (1980) have argued that their observation of a 22-year torsional wave pattern on the sun rules out present α-ω dynamo models. Such a pattern implies that the surface manifestations of the cycle are rooted in the deep layers of the sun and possibly associated with a primordial magnetic field. Our study indicates that the polarity reversal occurred first in the south for two consecutive cycles (19 and 20) then in the north in this cycle, and that the phase lag between hemispheres was 6 mo. to 1 yr. The former observation could be related to the fundamental solar magnetic cycle of 22 years, or two activity cycles. However, there is no way to account for such a persistent asymmetry in Babcock's model, where the magnetic field and solar activity evolve symmetrically with the field orientation mirrored about the equator. Yoshimura (1976) argues that in his dynamo model the two hemispheres are only weakly connected such that the maximum activity in one is not dependent on that of the other. But it would appear that solar cycle models are not yet sufficiently developed to completely explain the observations around the time of solar maximum.

ACKNOWLEDGEMENTS

The authors would like to thank R. Howard of the Mt. Wilson and Las Campanas Observatories for providing the magnetograph data, and A. Krieger for helpful discussions. We thank the AS&E and NOAA technical publication groups for their assistance with the figures. DFW and JMD were supported at AS&E by NASA Contracts NAS5-25496 and NASW-3586.

APPENDIX

Here we briefly describe the results of our observations of the development of southern hemisphere coronal holes of negative (new-cycle) polarity obtained from the Harvard OSO-6 movie. This movie provides daily maps of the corona in the MgX (625Å) line at about 30 arc-sec spatial resolution from August 1969 through April 1970. Coronal holes are easily detected as low emission regions on these maps (Withbroe et al., 1971).

We observed on this movie the development of three negative polarity coronal holes which may have been the early coronal signature of the new-cycle polarity reversal in the southern hemisphere. Table A summarizes the development of the southern coronal holes in late 1969 and early 1970 in terms of their CMP date and longitude. The "MgX" hole at L ≈ 220° developed earliest (October 1969) and lived the longest ($\geq$ 7 rotations). By CR 1559 a spur from this hole extended to the pole at L = 210°. The other two holes had lower contrast but developed larger areas. The hole at L ≈ 20° was bounded in the south by the polar crown until CR 1560 when an extensive hole from 345° to 250° appeared to connect to the south pole. The hole at L ≈ 110° stretched across the central meridian on the day of the 7 March 1970 eclipse. Although not previously noted as a coronal hole in X-rays, EUV or white light synoptic data (Broussard et. al., 1978; Withbroe et al., 1971; HHH, respectively), this hole can be identified for at least four rotations in the OSO-6 movie.*

---

* This hole is not to be confused with the "high-latitude," positive-polarity holes on 7 March 1970 discussed by Broussard et al.

TABLE A

SOUTHERN CORONAL HOLES OF NEGATIVE POLARITY: 1969-1970

CH	CMP Date	CMP L	C.R.
"L ~ 220°	14 Oct 1969	210°	1553
	11 Nov 1969	210	1154
	8 Dec 1969	210	1555
	5 Jan 1970	200	1556
	30 Jan 1970	230	1557
	27-28 Feb 1970	220-230	1558
	25 Mar 1970	250	1559
	28 Mar 1970[1]	210	1559
"L ~ 20°" [2]	22 Dec 1969	30°	1555
	20 Jan 1970	10	1556
	16 Feb 1970	15	1557
	15 Mar 1970	20	1558
	14-21 Apr 1970[3]	345-250	1559-1560
"L ~ 110°" [2]	13 Jan 1970	100°	1556
	8 Feb 1970	120	1557
	8 Mar 1970	110	1558
	4-5 Apr 1970	100-120	1559

Notes:

[1] By this rotation, the hole covered a large area in both latitude and longitude and was centered about L = 250°. Its southern-most extension lay near or at the south pole, was very dark and was at L = 210°.

[2] Both of these holes may have existed at CMP on their previous rotation, but their identification on the MgX maps is uncertain.

[3] The hole was extensive in longitude and probably connected to the south pole by this rotation.

TABLE I

POLAR EVENTS ASSOCIATED WITH SUNSPOT MAXIMUM

Cycle No.	Pole[1]	Sunspot Peak[2]	Polarity Reversal Above 70° Lat.	Mid-latitude Hole Appearance	Polar Crown Disappearance	Polar Hole Encirclement
21	N	July-Nov. 1979 1684-88[3]	Mar. 1980 1692-93 (Feb.-Mar. 1982 1719)	Dec. 1979-Jan. 1980 1690 May 1980 1695	Oct.-Nov. 1980 1701	July-Sept. 1981 1711-12
	S	Mar.-July 1980 1692-97	Sept 1980 1699	May 1980 1695 Nov.-Dec. 1981 1715	Apr.-May 1981 1707	June 1981-Jan. 1982 1710-16
20	S	Oct 1969 1553	Sept. 1969 1552	$\geq$ Oct. 1969 $\geq$ 1553	May 1970 1561	Mar. - Apr. 1970 1558-59
	N	June 1970 1562	July 1970[4] 1563 (Aug. 1971 1577)	$\leq$ May 1970[5] $\leq$ 1561 Jan 1971 1570	Sept. 1969[6] 1552 June-July 1971 1576	Mar.-Apr. 1971[7] 1572-73
19	S	Aug. 1957	Mar.-July 1957[8]	--	Jan. 1959[9]	--
	N	Jan. 1959	Nov. 1958[8]	--	Oct. 1959[9]	--

Notes to Table I:

(1) The first pole listed in each cycle switched polarity earliest.

(2) Peak in each hemisphere. Data for cycles 19 and 20 are from White and Trotter (1977). Data for cycle 21 were derived from NOAA-SESC sunspot group numbers (see text).

(3) Carrington Rotation number.

(4) From Howard (1974). The earliest time was the first reversal to positive polarity. The second time was the "final" reversal to positive polarity.

(5) From the data of Hundhausen et al. (1981). The earliest time is our estimate of the hole's original time of formation. The last time is HHH's time when the hole "reformed."

(6) The earliest time was when the polar crown preceeding positive polarity disappeared. The second time was when the "final" polar crown preceeding positive polarity disappeared.

(7) From the data of HHH.

(8) From Babcock (1959).

(9) Estimated from Waldmeier (1981); Figure 5.

TABLE II

LAG TIMES FROM POLAR POLARITY REVERSAL
(Carrington Rotations)

Cycle No.	Pole	Mid-Latitude Hole Appearance	Polar Crown Disappearance	Polar Hole Encirclement
21	N	-3 to +3	+(8 to 9)	+(18 to 20)
21	S	-4 +8	+(11 to 17)	
20	S	≥ +1 +9	+(6 to 7)	
20	N	≥ -2 to +7	+13	+(9 to 10)
19	S	-- +(20 to 25)	--	
19	N	-- +12	--	

REFERENCES

Babcock, H. D.: 1959, Astrophys. J. 130, 364.

Babcock, H. D.: 1961, Astrophys. J. 133, 572.

Babcock, H. D.: 1963, in L. Goldberg (ed.) Ann. Rev. Astron. Astrophys. 1, Annual Reviews, Inc., Palo Alto, California.

Bohlin, J. D. and Sheeley, N. R., Jr.: 1978, Solar Phys. 56, 125.

Broussard, R. M., Sheeley, N. R., Jr., Tousey, R. and Underwood, J.H.: 1978, Solar Phys 56, 161.

Hansen, S. F. and Hansen, R. T.: 1977, Solar Phys. 51, 169.

Howard, R.: 1972, Solar Phys. 25, 5.

Howard, R.: 1974, Solar Phys. 38, 283.

Howard, R. and LaBonte, B. J.: 1980, Astrophys. J. 239, L33.

Howard, R. and LaBonte, B. J.: 1981, Solar Phys. 74, 131.

Hundhausen, A. J.: 1977, in J. Zirker (ed.) Coronal Holes and High-Speed Wind Streams, Colorado Associated Univ. Press, Boulder, Colorado.

Hundhausen, A. J., Hansen, R. T. and Hansen, S. F.: 1981, J. Geophys. Rev. 86, 2079.

Kahler, S. W., Davis, J. M. and Harvey J. W.: 1983, Solar Phys. (submitted).

Krieger, A. S., Vaiana G. S. and van Speybroeck, L. P.: 1971, in R. Howard (ed.) Solar Magnetic Fields, D. Reidel, Dordrecht, Holland.

Krieger, A. S., Timothy, A. F. and Roelof, E. C.: 1973, Solar Phys. 29, 505.

Leighton, R. B.: 1964, Astrophys. J. 140, 1547.

McIntosh, P. S.: 1972a, Rev. Geophys. Space Phys. 10, 837.

McIntosh, P. S.: 1972b, in P. S. McIntosh and M. Dryer (eds.) Solar Activity Observations and Predictions, MIT Press, Cambridge, MA.

McIntosh, P. S.: 1979, UAG Report 70, World Data Center A for Solar-Terrestrial Physics, NOAA, Boulder, Colorado.

McIntosh, P. S.: 1980, in M. Dryer and E. Tandberg-Hanssen (eds.) Solar and Interplanetary Dynamics, D. Reidel, Dordrecht, Holland.

McIntosh, P. S. Krieger, A. S., Nolte, J. T. and Vaiana, G.: 1976, Solar Phys 49, 57.

Nolte, J. T., Davis, J. M., Gerassimenko, M., Lazarus, A. J. and Sullivan, J. D.: 1977, Geophys. Res. Lett. 4, 291.

Sheeley, N. R., Jr.: 1980, Solar Phys 65, 229.

Sheeley, N. R., Jr., Asbridge, J. R., Bame, S. J. and Harvey, J. W.,: 1977, Solar Phys 52, 1977.

Solar Geophysical Data Bulletins, U.S. Department of Commerce, NOAA, Boulder, Colorado.

Topka, K., Moore, R., LaBonte, B. J., and Howard, R.: 1982, Solar Phys. 79, 231.

Van Speybroeck, L.P., Krieger, A. S. and Vaiana, G. S.: 1970: Nature 227, 818.

Waldmeier, M.: 1973, Solar Phys. 28, 389.

Waldmeier, M.: 1981, Solar Phys. 70, 251.

White, O. R. and Trotter, D. E.: 1977, Astrophys. J. Suppl. 33, 391.

Withbroe, G. L.: 1981, private communication of 16-mm OSO-6 movie.

Withbroe, G. L., Dupree, A. K., Goldberg, L., Huber, M. C. E., Noyes, R. W., Parkinson, W. H. and Reeves, E. M.: 1971, Solar Phys. 21, 272.

Yoshimura, H.: 1976, Solar Phys. 47, 581.

FIGURE CAPTIONS

Figure 1 - The rise, maximum and early decline phases of solar sunspot cycles 20 (bottom curve) and 21 (top). The curves show smoothed values of R_z, the Zurich sunspot number, normalized to their starting minima in October 1964 (bottom) and June 1976 (top). The dashed line represents predicted R_z through late 1982 and early 1983. These data are adapted from the Solar-Geophysical Data Bulletin. The vertical lines denote the times of AS&E X-ray rocket flights (there were 2 in November 1979), and the box at the bottom indicates the time coverage of the Harvard OSO-6 MgX movie.

Figure 2 - A superposition of an AS&E X-ray image of the inner corona obtained during a rocket flight and a ground-based HAO white light image of the outer corona. Both were taken during the solar eclipse of 7 March 1970. The X-ray image had passbands of 3-30 and 44-55 Å. Solar north is at an angle of ____° CW from the top of the figure.

Figure 3 - Coronal data superimposed on an Hα synoptic chart for CR 1558 (McIntosh, 1979). (a) Boundaries of coronal holes drawn from the 7 March 1970 X-ray image in Figure 2. The three vertical lines represent the positions of the east limb (left), CMP (center) and west limb (right) on that day. Single dashed lines indicate uncertain boundaries; double dashed lines indicate the locations of coronal filament cavities. The "X"s mark the location of sunspots observed with the X-ray experiment, and provide a benchmark of the accuracy of transfering the X-ray data to the rectangular format. (b) The 2 and 3 x 10^{-8} pB contours of the white light K-corona adapted from the west limb synoptic data of HHH.

Figure 4 - Top: AS&E X-ray rocket images of the corona obtained on 7 November 1979 (a) and 13 February 1981 (c). The passbands of the images were 8 ≈ 100Å and 8-59, 44-64Å, respectively. Bottom: Tracings on Stonyhurst disks of the boundaries of the darkest areas on the 7 November 1979 (b) and 13 February 1981 (d) X-ray images. Dashed lines indicate less well defined boundaries. Also shown are the principle definite (solid lines) neutral lines and filaments transfered from the synoptic charts for CR 1688 and 1705.

Figure 5 - The southern high latitude zone through the maximum of cycle 21; i.e., CR 1682 - 1725 or May 1979 - Sept. 1982. This time series maps the patterns of magnetic polarity (white = positive, black = negative) as identified on Hα synoptic charts. Included on the maps are coronal hole boundaries (hatched areas) drawn from daily KPNO HeI-10830 images. This format repeats two 360° rotations/consecutive horizontally in order to better show the migration of large-scale features. The horizontal arrows mark the rotations during which the AS&E rocket images of Figure 4 were obtained.

Figure 6 - The variation of the northern (a) and southern (b) photospheric magnetic field strength averaged over six latitude intervals from 1978 through October 1982. The zero level is drawn for each latitude interval. The field averages are 27 day running means. The large excursions in the data above 70° are related to data gaps and instrument recalibrations at times when the respective poles had their maximum tilt away from the earth. These data are from Mt. Wilson Observatory courtesy of R. Howard.

C-2

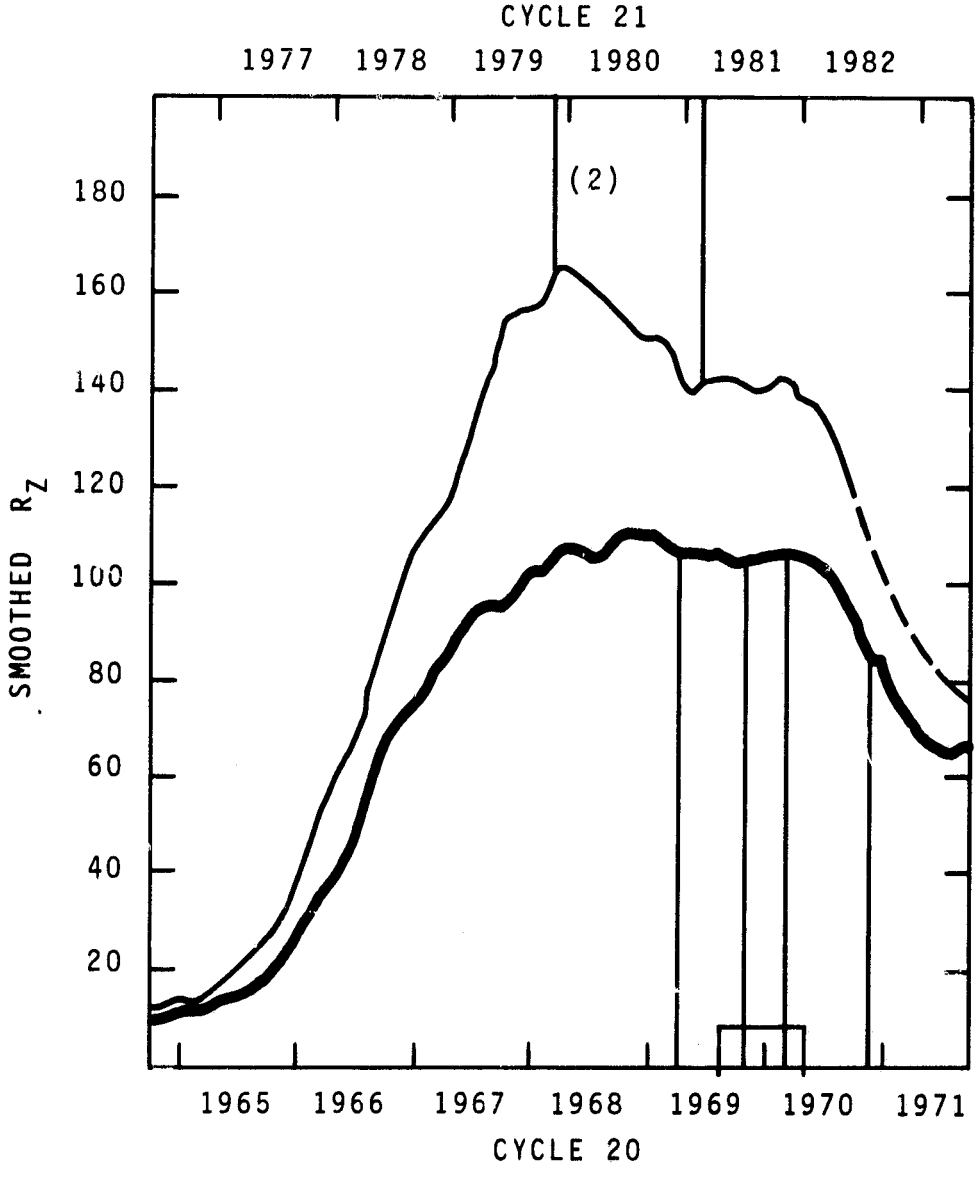
CYCLE 21
1977
1978
1979
1980
1981
1982
(2)
180
160
140
120
100
80
60
40
20
SMOOTHED R_Z
1965
1966
1967
1968
1969
1970
1971
CYCLE 20

Figure 1.

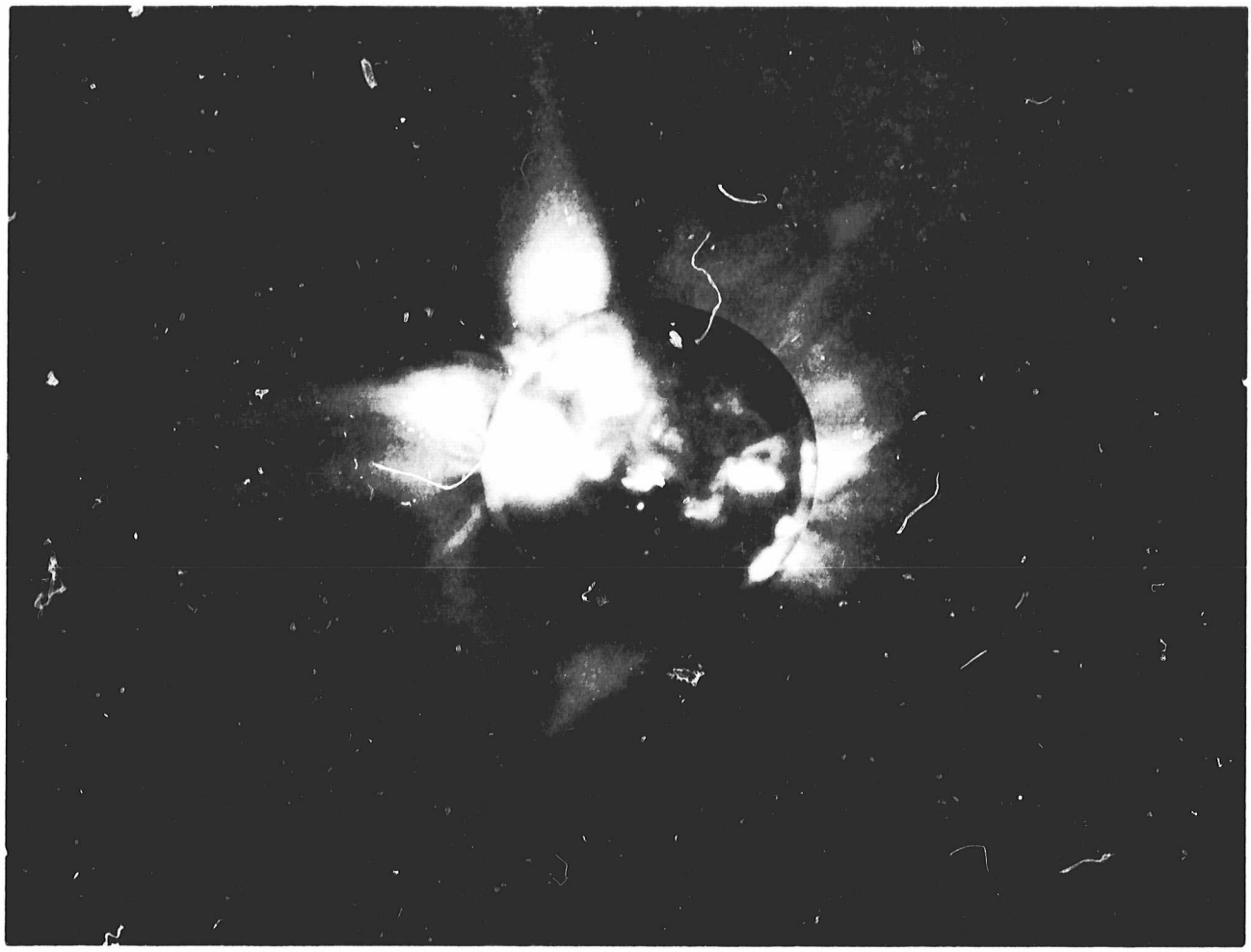

Figure 2.

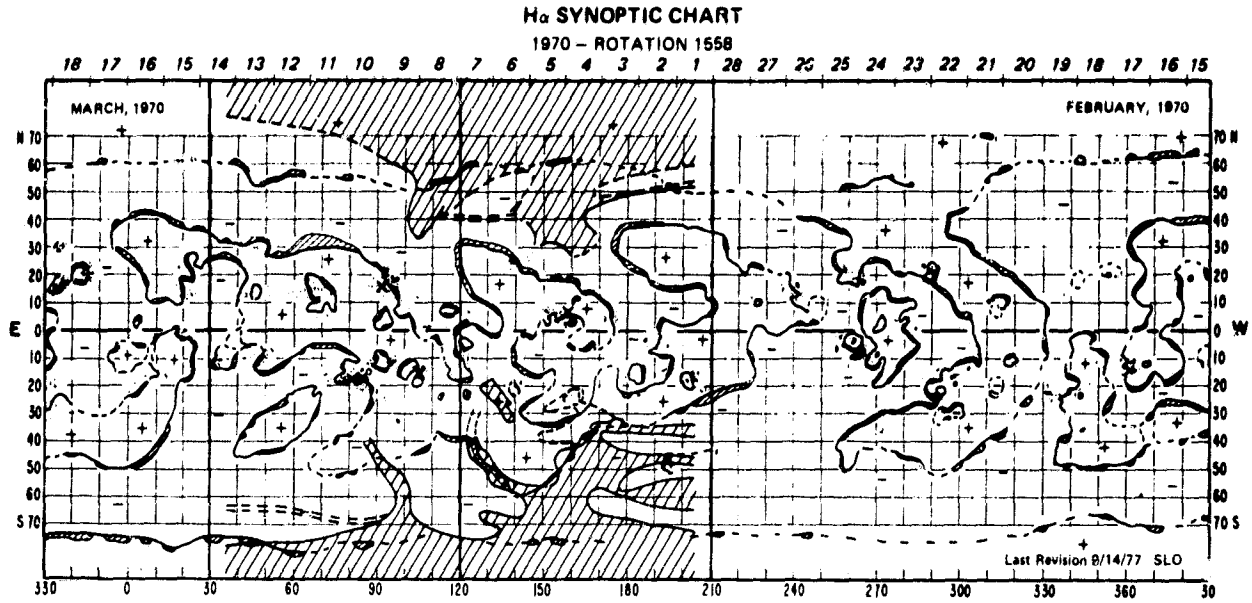

(a)

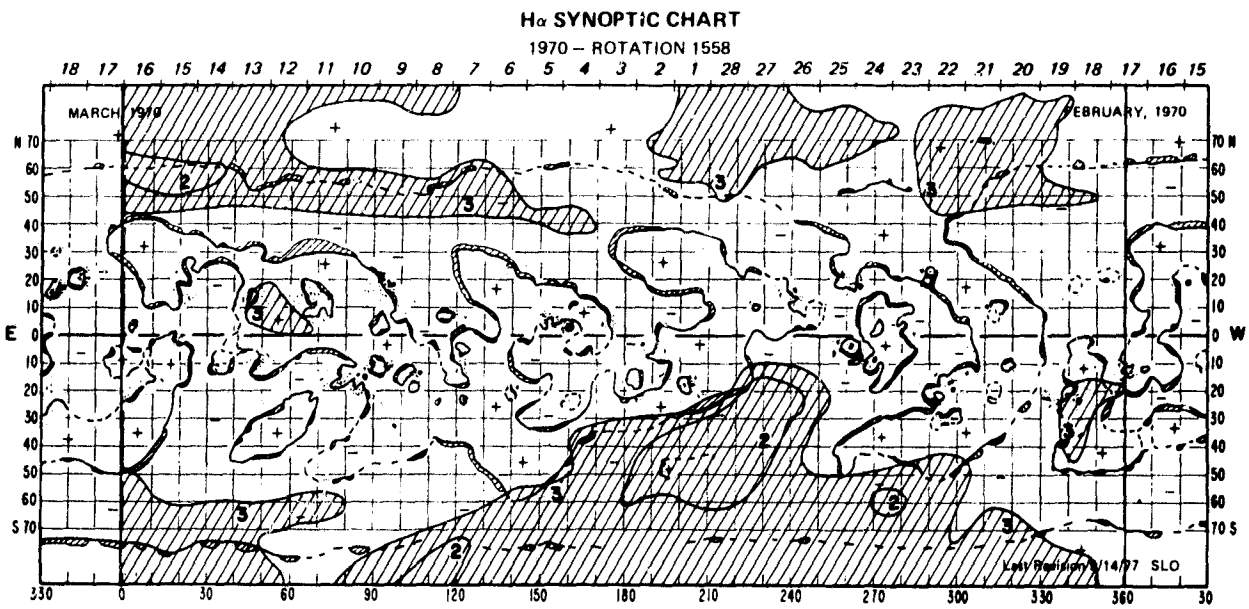

(b)

Figure 3.

7 NOVEMBER 1979

13 FEBRUARY 1981

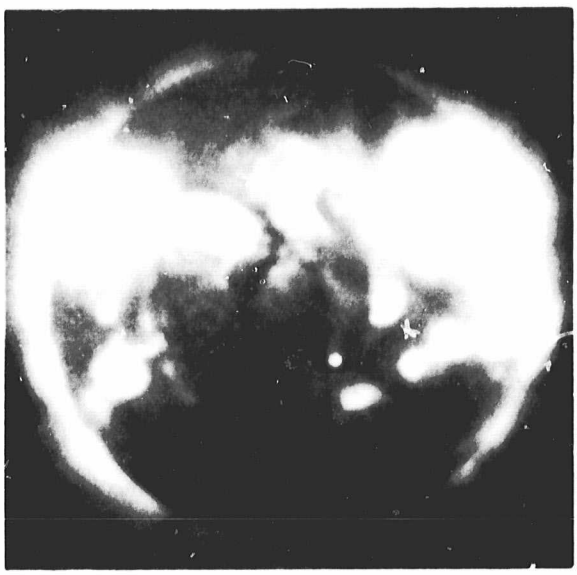

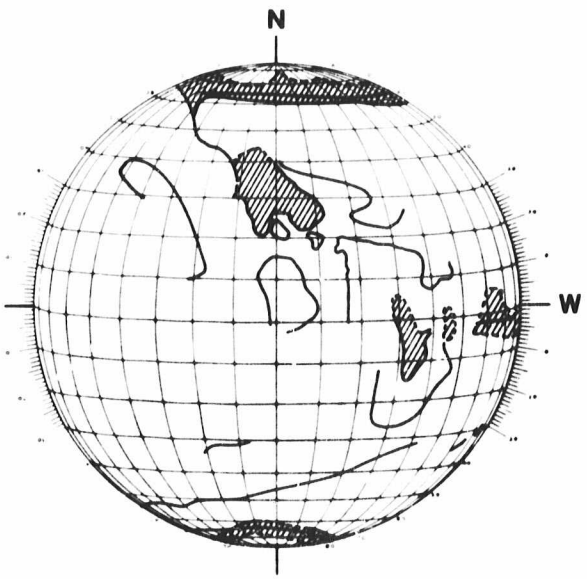

(b)

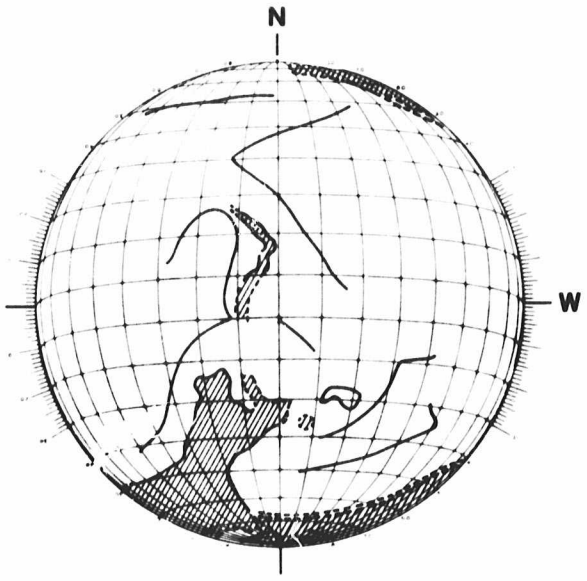

(d)

Figure 4.

SL-0814

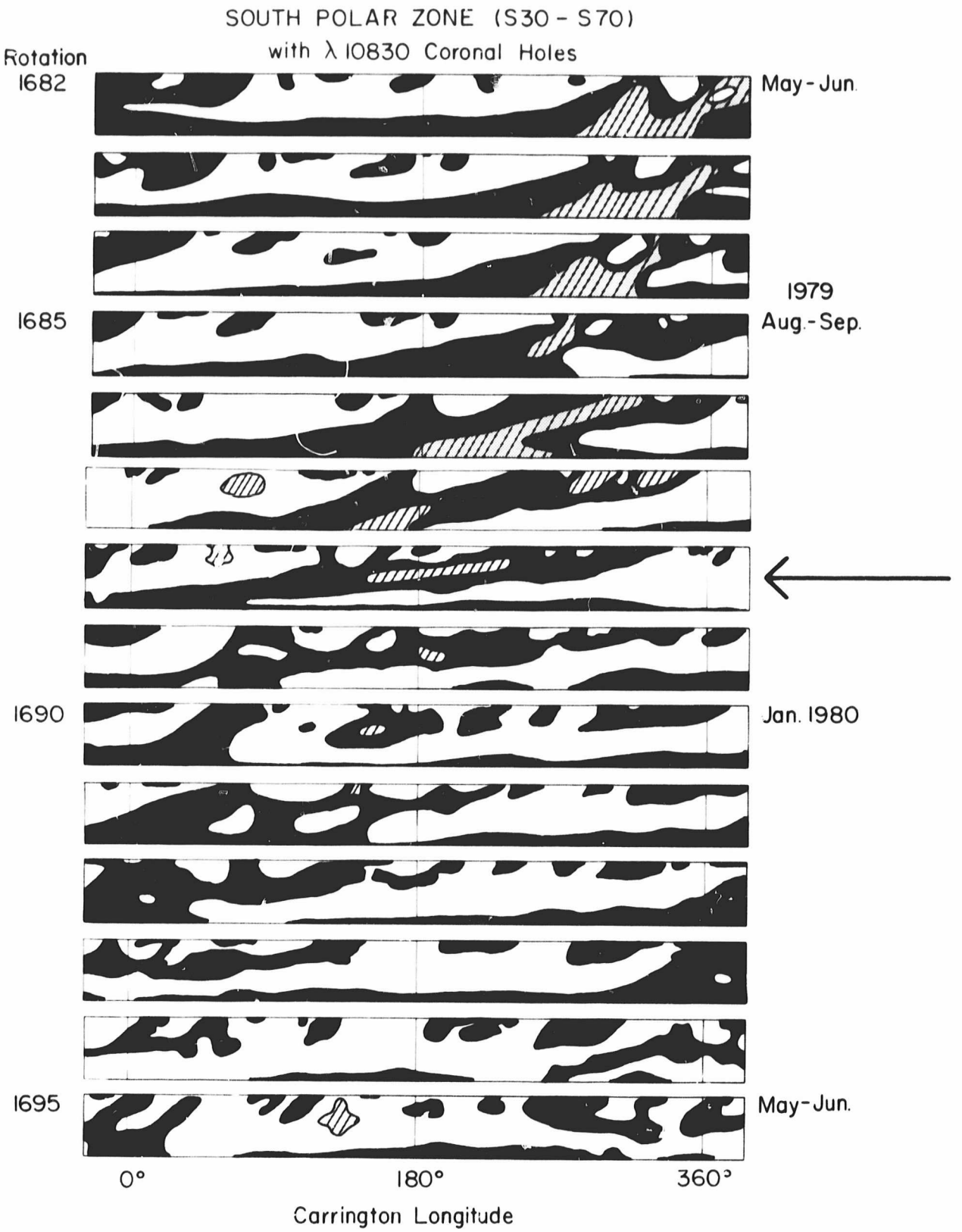

Figure 5a.

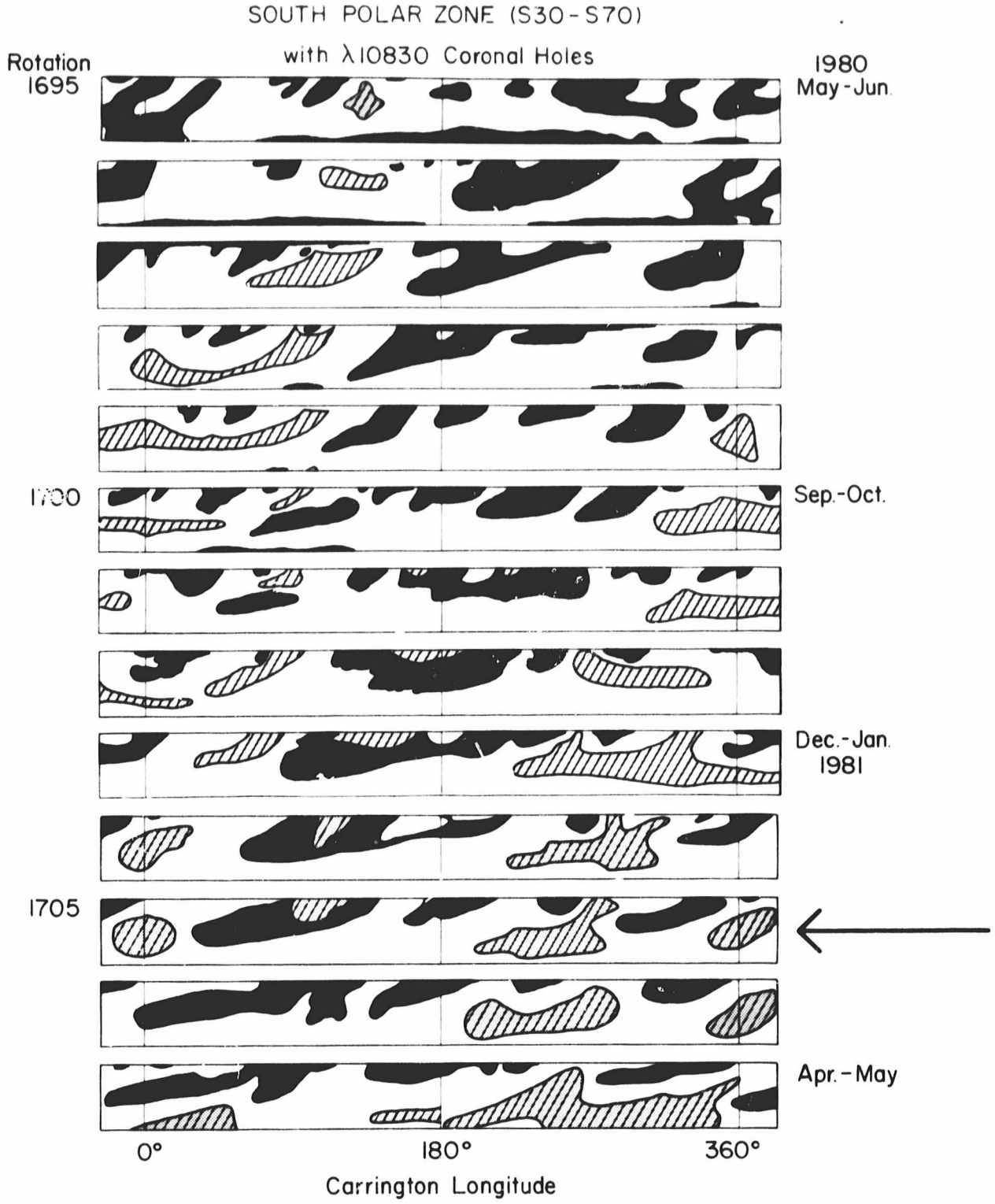

Figure 5b.

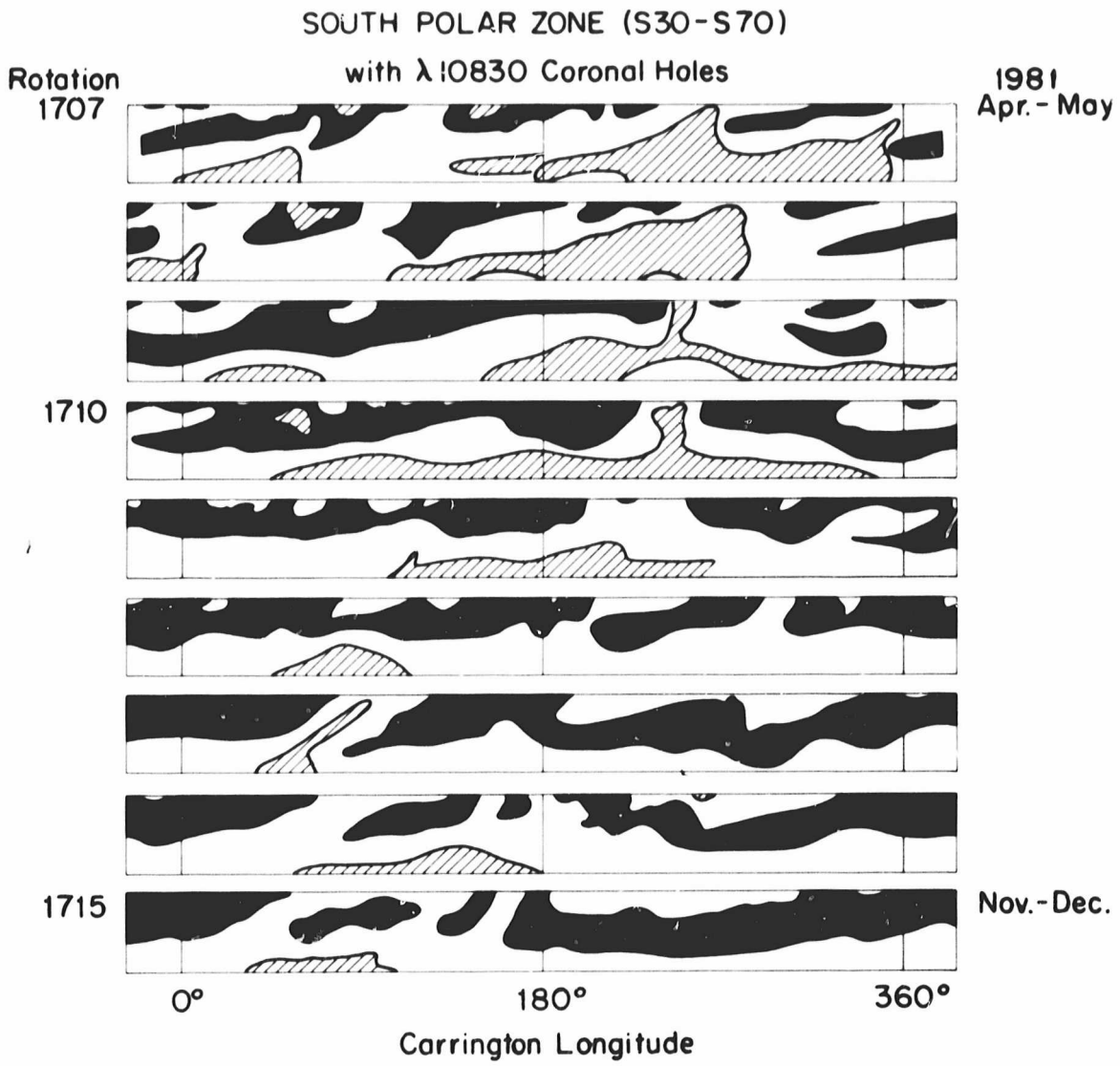

Figure 5c.

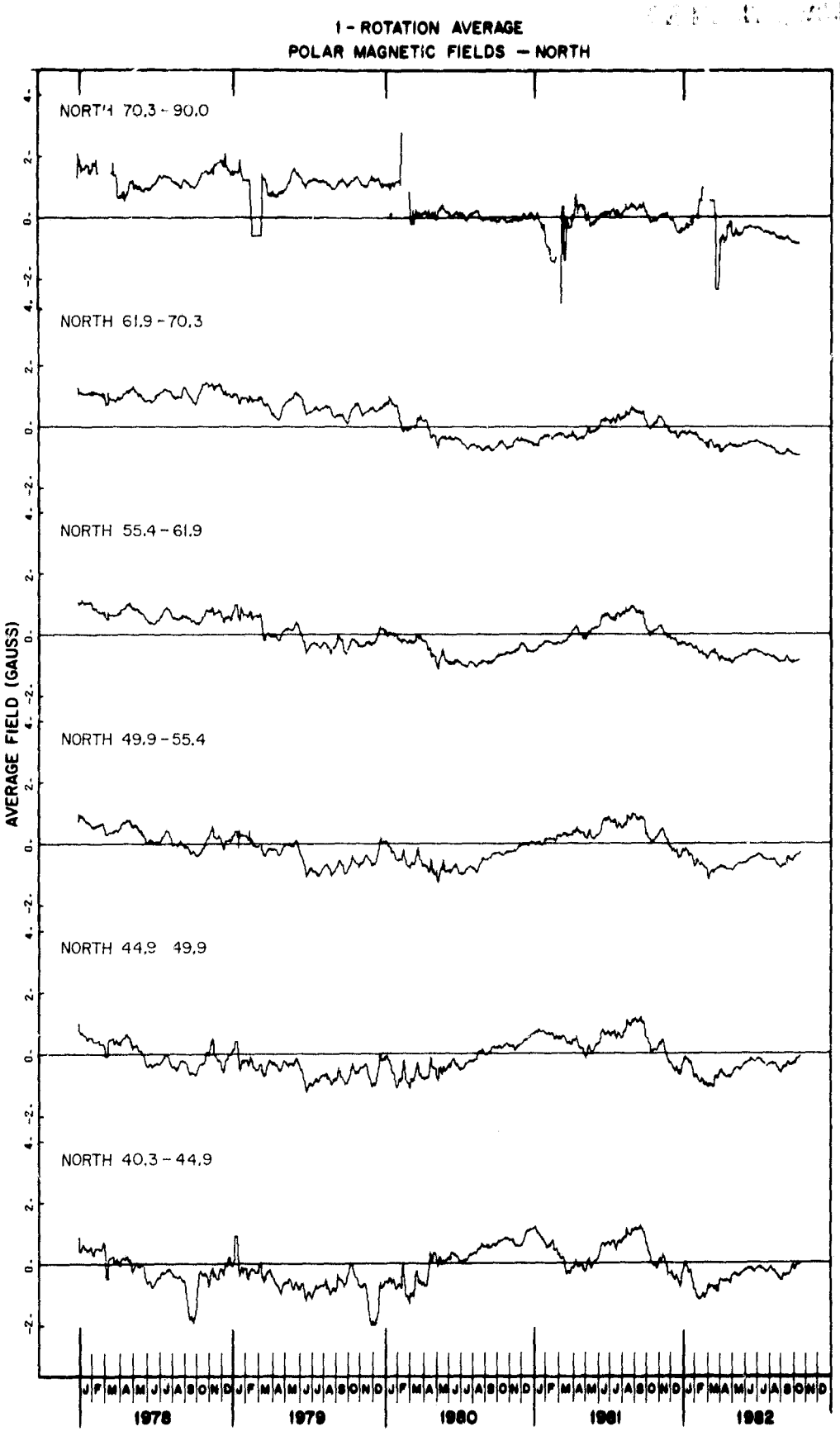
1 - ROTATION AVERAGE
POLAR MAGNETIC FIELDS — NORTH
NORTH 70.3 - 90.0
NORTH 61.9 - 70.3
NORTH 55.4 - 61.9
NORTH 49.9 - 55.4
NORTH 44.9 49.9
NORTH 40.3 - 44.9
AVERAGE FIELD (GAUSS)
4.
2.
0.
-2.
J F M A M J J A S O N D J F M A M J J A S O N D J F M A M J J A S O N D J F M A M J J A S O N D J F M A M J J A S O N D
1978
1979
1980
1981
1982

Figure 6a.

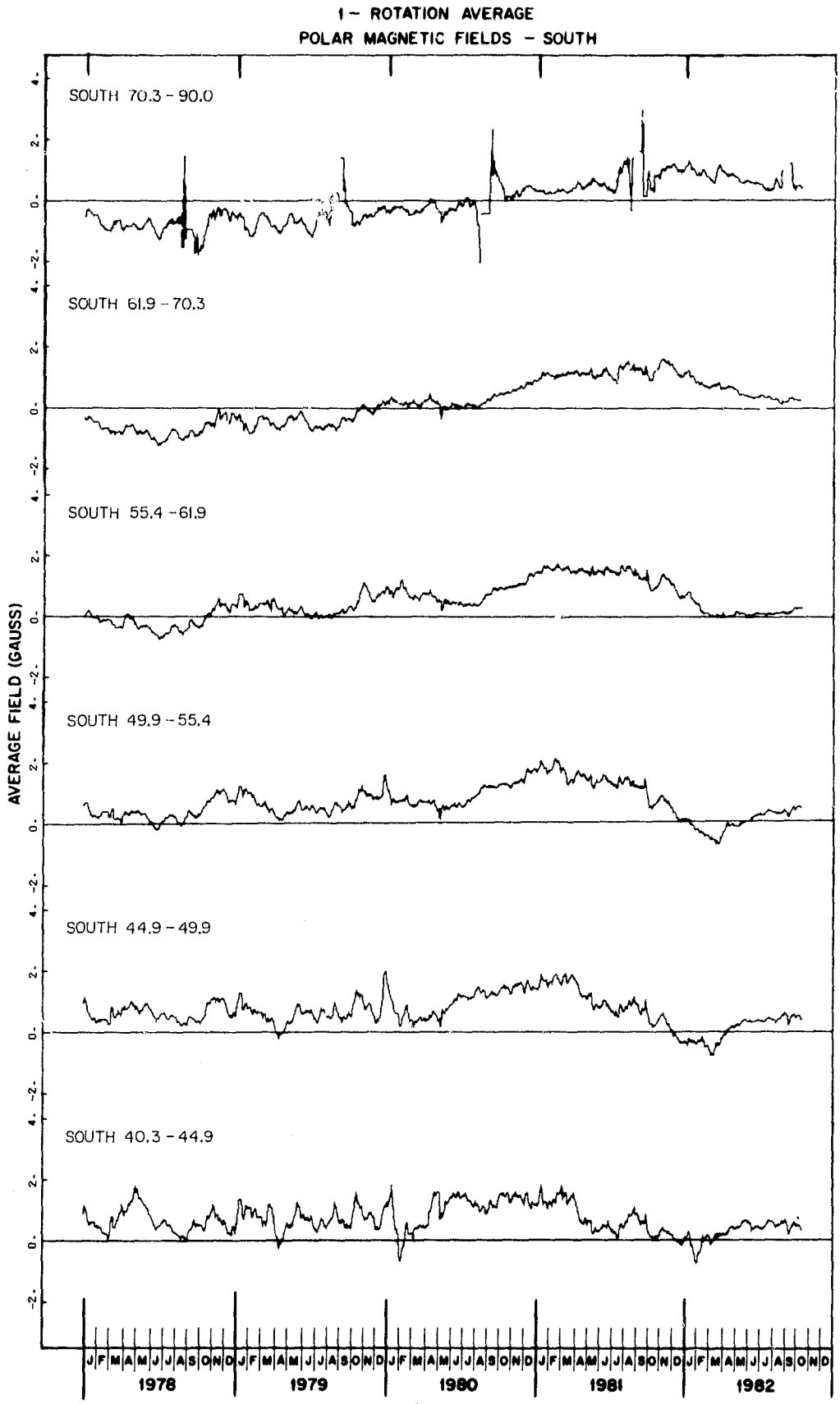
1 – ROTATION AVERAGE
POLAR MAGNETIC FIELDS – SOUTH
SOUTH 70.3 – 90.0
SOUTH 61.9 – 70.3
SOUTH 55.4 – 61.9
SOUTH 49.9 – 55.4
SOUTH 44.9 – 49.9
SOUTH 40.3 – 44.9
AVERAGE FIELD (GAUSS)
J F M A M J J A S O N D J F M A M J J A S O N D J F M A M J J A S O N D J F M A M J J A S O N D J F M A M J J A S O N D
1978
1979
1980
1981
1982

Figure 6b.

APPENDIX: AS&E DOCUMENTATION

During the performance of the contract ten monthly progress reports were submitted to NASA. These reports are indexed as follows:

Report No. 1	ASE-4720	31 March - 30 April 1982
2	ASE-4727	1 - 31 May 1982
3	ASE-4732	1 - 30 June 1982
4	ASE-4741	1 - 31 July 1982
5	ASE-4748	1 - 31 August 1982
6 and 7	ASE-4764	1 September - 31 October 1982
8	ASE-4771	1 - 30 November 1982
9 and 10	ASE-4780	1 December 1982 - 31 January 1983